

# Investigation of the interior RC beam-column joints under monotonic antisymmetrical load

Fei GAO<sup>a</sup>, Zhiqiang TANG<sup>a</sup>, Biao HU<sup>b\*</sup>, Junbo CHEN<sup>c</sup>, Hongping ZHU<sup>a</sup>, Jian MA<sup>a</sup>

<sup>a</sup> School of Civil Engineering and Mechanics, Huazhong University of Science and Technology, Wuhan 430074, China

<sup>b</sup> Guangdong Provincial Key Laboratory of Durability for Marine Civil Engineering, Shenzhen University, Shenzhen 518060, China

<sup>c</sup> Department of Civil and Environmental Engineering, The Hong Kong Polytechnic University, Hong Kong 999077, China

\*Corresponding author. E-mail: biao3-c@szu.edu.cn

© Higher Education Press and Springer-Verlag GmbH Germany, part of Springer Nature 2019

**ABSTRACT** The paper presents numerical findings of reinforced concrete interior beam-column joints under monotonic antisymmetrical load. The finite element models considered compression and tension damage were calibrated by test results in terms of the load-displacement, failure modes, and strains of longitudinal steel. The emphasis was put on studying the effects of hoop reinforcement ratio in joint core and the axial compression ratio on the responses of the joints. The results show that, in addition to the truss and strut-and-tie mechanisms, the confinement mechanism also existed in the joint core. A certain amount of stirrup is not only able to enhance the confinement in joint core, undertake a part of shear force and thus to increase the shear capacity, prevent the outward buckling of steel bars in column, improve the stress distribution in joint core, delay cracking and restrain the propagation of cracks, but also to increase the yield load, decrease the yield displacement of beam and improve the joint ductility. However, excessive horizontal stirrups contribute little to the joint performance. In a certain range, larger axial compression ratio is beneficial for the joint mechanical behavior, while it is negative when axial compression ratio is too large.

**KEYWORDS** RC beam-column joint, reinforcement ratio in joint core, axial compression ratio, finite element, test

## 1 Introduction

Over past decades, great accomplishments have been achieved in uncovering mechanical mechanisms, modeling shear strength, and updating seismic resistant design of reinforced concrete (RC) beam-column joints. Nevertheless, due to the complex stress distribution in joint core and adjacent areas of a RC beam-column joint, consensus hasn't yet been reached in understanding this critical problem. Truss-based analogy [1,2] and strut-and-tie model [3–5] are two typical models for analyzing the joint mechanical mechanisms with high recognition. Although these two theories have provided excellent conceptual tools to approximately visualize the internal forces transfer in joint core [6–8], it is believed that they cannot comprehensively consider the effect of stirrups on the structural behavior of RC beam-column joints and the

detailed responses in joint adjacent areas, such as the beam end zone [9,10].

A great number of experimental studies about the mechanical behavior of RC beam-column joints have been conducted in research community. Based on those valuable results, various international design codes have been established [11–14]. According to the methods for determination of the stirrup quantity demanded, the current codes can be classified into two categories. One obtains the amount of stirrups in joint core as per shear strength model based on standard truss model [11]. The other is based on the strut-and-tie model, which emphasizes that it only needs to control the maximum shear compression ratio and determines the design of stirrups according to the minimum hoop reinforcement ratio [12]. By comparing various codes [11–14], it is found that the hoop reinforcement ratio in joint core region varies in different codes. A more detailed critical review of international design codes of RC beam-column joints are available elsewhere [6–8,10].

Great efforts have been made in understanding the effect of hoop reinforcement ratio in joint core [3,15–18]. It was found that further increase in hoop reinforcement ratio in joint core has a very limited effect on improving the joint shear strength when the reinforcement ratio larger than 0.45% and 0.55%, respectively [19]. However, Kim and LaFave [9] and Haach et al. [20] quantitatively emphasized the effect of stirrups on the distribution of stress-strain states.

Current codes and research results also showed discrepancies in comprehending the influences of axial load ratio on RC beam-column joints. As per Eurocode 8 [13] and NZS 3101 [11], when the joint attains the equivalent seismic ductility level, the higher axial load ratio is, the less the amount stirrups require. However, ACI 318-08 [12] ignores the influences of axial load ratio in design. Some researchers believed that axial load ratio shows little influence on joint performance [9], whereas others favored that it does [6,7,9,16,21].

Over years, the study of RC beam-column joints has relied mainly on experimental tests. Compared with large numbers of tests, fewer investigations are available by means of finite element (FE) method [16,20,22–24]. For modeling of RC, the damage of concrete should be considered [25,26] to achieve more accurate results and stochastic analysis is recommended to demonstrate the results are reproducible [27–29]. Rabczuk and his colleagues have been working on modeling of RC and evolution of cracking by means of various advanced methods, e.g., FE method [30], meshfree method [31,32], particle method [33,34], partition of unity method [35], coupled element free Galerkin/FE approach [36], and cohesive crack method [37]. Based on those significant and valuable investigations, a series of highly-acknowledged results and novel findings have been contributed by Rabczuk and his colleagues.

During the past 60 years, most of the research focused on behavior of RC beam-column joints under seismic loading. However, compared with cyclically loaded joints, very little information are reported in literature for the monotonically loaded RC joints [20,21,38–41]. Actually, remarkable differences exist in the design of joints for seismic loading or monotonic loading [19,20]. Considering the fact that the function of joint core stirrups has not been fully understood and controversy still exists with regard to the influences of joint hoop reinforcement ratio and axial load ratio, this paper systematically carried out a series of three-dimensional FE analysis on RC beam-column interior joints under monotonic antisymmetrical load. By analyzing reinforcement strain in joint core and adjacent regions, the role of joint hoop stirrups in force transfer mechanism, the influences of axial load ratio and joint hoop reinforcement on structural responses of joint were further investigated.

## 2 Description of test program

### 2.1 Test specimens

Three RC interior beam-to-column joint specimens, with specimen identity (ID) of SP1, SP2, and SP3, were designed according to Chinese Concrete Code [14]. Table 1 summarizes the general information for those specimens. Three different kind of longitudinal reinforcement (HRB 335, HRB500E, and HRB600) were used in SP1, SP2, and SP3, respectively. The letters HRB represent an abbreviation of the hot-rolled ribbed bar and the figure represents the nominal tensile strength of steel bar. For example, HRB600 means the steel bar is hot-rolled ribbed bar with a yield strength of 600 MPa. The reinforcement details and geometrical properties of those three joints are shown in Fig. 1. Specimens SP2 and SP3 had identical reinforcement layout but the former reinforced with HRB500E and the latter with HRB600. The targeted concrete compressive strength for all specimens was designed to be grade C50 (compressive strength = 50 MPa). The average value of three concrete cubes was used to determine the compressive strength of concrete of each specimen on the exact day the joint test was conducted. The material properties of concrete and steel reinforcing bars are summarized in Table 2.

### 2.2 Test setup and procedure

Each specimen was subjected to monotonic antisymmetrical loads applied at beam tips, and a constant axial load with magnitude of  $0.3f_c' A_g$  (axial load ratio  $\nu = 0.3$ ) was applied on the column of each specimens throughout the test (Fig. 2). The load was applied in a displacement control mode at the rate of 0.005 mm/s. Linear variable differential transformer (LVDTs) were used to measure the transverse deflection at point where the loads applied. Strain gauges were placed on both the longitudinal and transverse reinforcing steels at selected locations within and around the beam-column joints. The load-displacement responses, strain data and cracking modes were then used to analyze the structural behavior of the beam-column joints and to calibrate the FE models. The test setup, positioning the strain gauges and the LVDTs are shown in Figs. 1 and 2.

## 3 FE modeling

### 3.1 General

FE models have been developed using commercial software ABAQUS [42] to carry out numerical analyses. The nonlinearity of concrete and reinforcement as well as

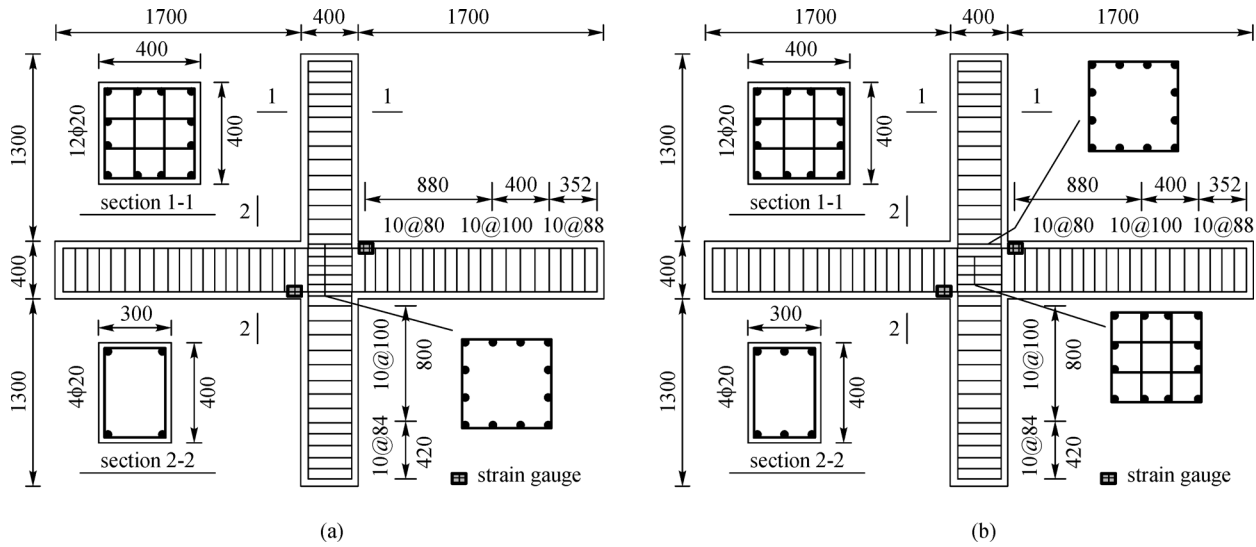


Fig. 1 Details of test specimens. (a) SP1; (b) SP2 and SP3.

Table 1 General information of RC interior beam-to-column joints specimens

specimens	longitudinal steel bar	beam, longitudinal steel bar (one side)	column, longitudinal steel bar	transverse reinforcement ratio in joint core		axial load ratio $\nu$	shear compression ratios $\lambda$	$\frac{M_{cu}}{M_{bu}}$
				number $N$	$\rho_{svj}$			
SP1	HRB335	2Φ20	12Φ20	6Φ10	1.03%	0.3	0.12	4.95
SP2	HRB500E	3Φ20	12Φ20	6Φ10 + 8Φ10	1.72%	0.3	0.27	2.27
SP3	HRB600	3Φ20	12Φ20	6Φ10 + 8Φ10	1.72%	0.3	0.32	1.90

Note: Volume reinforcement ratio of joint core is calculated as  $\rho_{svj} = \frac{\sum n_1 A_{sv1} L_1 + \sum n_2 A_{sv2} L_2}{b_j h_j h_b}$ , in which  $b_j$  and  $h_j$  are the effect width and height of the horizontal shear plane in joint core, respectively;  $n_1$ ,  $A_{sv1}$ , and  $L_1$  are the number of transverse bars along the direction of  $b_j$  in joint core, the cross section area, and length of one transverse bar, respectively;  $n_2$ ,  $A_{sv2}$ , and  $L_2$  are the number of transverse bars along the direction of  $h_j$  in joint core, the cross section area, and length of one transverse bar, respectively. Axial compression ratio is defined as  $\nu = \frac{N}{f_c b_c h_c}$ , in which  $N$  is the design value of axial force on column,  $f_c$  is the compression strength of concrete,  $b_c$  is the width of column cross section, and  $h_c$  is the height of column cross section. Shear compression ratio is defined as  $\lambda = \frac{v_{jh}}{f_c b_j h_j}$ , in which  $v_{jh}$  is design value of horizontal shear force in joint core.  $M_{cu}$  and  $M_{bu}$  are the design values of ultimate moment of column and beam.

damage conditions of concrete under tension and compression were taken into account to accurately capture the behavior of the RC interior beam-to-column joints. Test results of the three interior beam-to-column joints described in Section 2 were used for FE models validation.

### 3.2 Element types, boundary conditions, and loading conditions

The eight-node hexahedral solid element with reduced integration (C3D8R) and the two-node linear displacement truss element (T3D2) were adopted to simulate the behavior of concrete and steel bars, respectively. The reinforcements were embedded into concrete, which means the reinforcements are fully bonded to the surrounding concrete [43]. The interaction of concrete and steel bars are considered in the FE model by using tension stiffening, which is a generally accepted modeling technique in simulating the behavior of RC beam-column

joints [20,44–53]. The boundary conditions and loading directions are shown in Fig. 2. In FE model, the vertical and horizontal displacements of column bottom and only horizontal movement of the column top were restrained. Both the beam ends were free for applying transverse loads. Although the exact boundary conditions of the test specimens cannot be accurately modeled, this slight bias of simulating the boundary conditions imposes rather limited influence on the response of full-scale RC concrete components and structures [27,43]. A constant axial compressive load was applied at the top of the column while antisymmetrical vertical loads were applied to beam tips by means of displacement control manner.

### 3.3 Material modeling

The elasticity-ideal plasticity-hardening plasticity model as shown in Fig. 3 was adopted for modeling the steel reinforcement. The measured material properties including

**Table 2** Materials properties

specimen	steel bar					concrete		
	grade	yield strength $f_y^0$ (MPa)	yield strain $\epsilon_y^0$	tensile strength $f_{ts}^0$ (MPa)	Young's modulus $E_s^0$ (GPa)	grade	compression strength $f_{cu}^0$ (MPa)	tensile strength $f_{tc}^0$ (MPa)
SP1	HRB335	427.5	0.0021	548.5	204	C50	48.4	3.3
SP2	HRB500E	543.9	0.0028	703.7	197	C50	48.8	3.4
SP3	HRB600	607.8	0.0031	774.1	194	C50	49.1	3.7

Note:  $f_{cu}^0$  and  $f_{tc}^0$  are the compression and tension strength of concrete based on concrete cube tests.

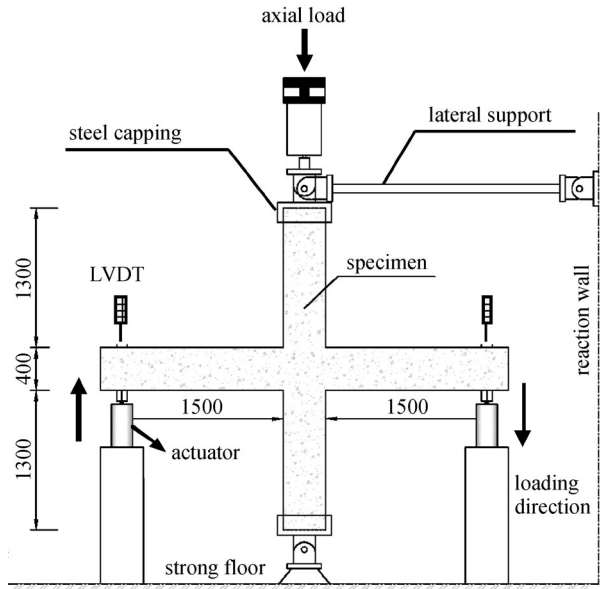


**Fig. 2** Test setup.

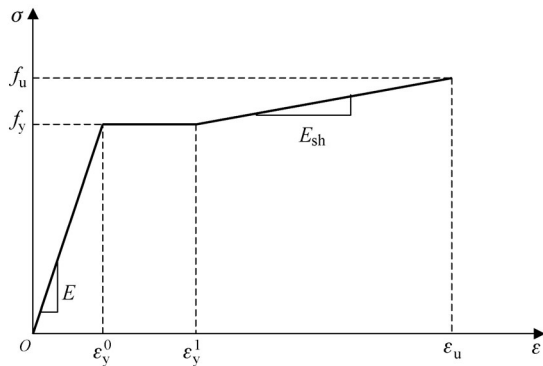


**Fig. 3** Steel constitutive model.

elastic modulus ( $E$ ), yield strength ( $f_y$ ), ultimate strength ( $f_u$ ), yield strain ( $\epsilon_y^0$ ), strain that hardening initiates ( $\epsilon_y^1$ ), and hardening modulus  $E_{sh}$  were used. The Poisson's ratio ( $\nu$ ) of steel materials was set to 0.3.

The concrete damaged plasticity (CDP) model was adopted to model the nonlinear behavior of concrete. CDP model in ABAQUS was developed based on the model proposed by Lubliner et al. [54]. In this model, key

parameters are required to define the concrete behavior under tri-axial stress states, namely the dilation angle ( $\psi$ ), the flow potential eccentricity ( $e$ ), the viscosity parameter ( $\mu$ ), the ratio of compressive strength under biaxial loading to the uniaxial compressive strength ( $f_{b0}/f_c'$ ), and the ratio of the second stress invariant on the tensile meridian to that on the compressive meridian ( $K_c$ ). Regarding the values of  $e$ ,  $f_{b0}/f_c'$ , and  $K_c$ , default values recommended by ABAQUS were utilized, namely  $e = 0.1$ ,  $f_{b0}/f_c' = 1.16$ , and  $K_c = 2/3$ . For the dilation angle ( $\psi$ ), a value of  $35^\circ$  was adopted [55,56].

Regarding the elasticity of the concrete model, the Poisson ratio  $\nu$  was set to 0.2 and the Young's modulus  $E_0$  was given in accordance with Chinese code [57] based on the measured concrete compressive cube strength. The stress-strain relationships of concrete under tension and compression are required by the CDP model apart from the aforementioned parameters. The constitutive models proposed by Guo [58] were adopted and typical stress-strain curves under tension and compression are shown in Fig. 4.

The stress-strain relation under uniaxial compression is expressed by Eq. (1).

$$\frac{\sigma_c}{f_c} = \begin{cases} \alpha_a x + (3 - 2\alpha_a)x^2 + (\alpha_a - 2)x^3, & x = \frac{\epsilon_c}{\epsilon_{c0}} < 1, \\ \frac{x}{\alpha_d(x-1)^2 + x}, & x = \frac{\epsilon_c}{\epsilon_{c0}} \geq 1, \end{cases} \quad (1)$$

where  $f_c$  is concrete compressive strength taken as the cylinder strength converted from the measured cube strength in accordance with Chinese code [57];  $\epsilon_c$  is the concrete uniaxial compressive strain;  $\sigma_c$  is the corresponding stress when concrete strain is  $\epsilon_c$ ;  $\epsilon_{c0}$  is the corresponding strain of concrete compressive strength and was taken as 0.002 [56,59,60]; and  $\alpha_a$  and  $\alpha_d$  denote the coefficients to determine the ascending and descending portions of concrete stress-strain curve under uniaxial compression and were set to 1.78 and 2.48, respectively.

When referring to the uniaxial tensile behavior of concrete, relation described by Eq. (2) was adopted.

$$\frac{\sigma_t}{f_t} = \frac{x}{\alpha_t(x-1)^{1.7} + x}, \quad x = \frac{\epsilon_t}{\epsilon_{t0}} \geq 1, \quad (2)$$

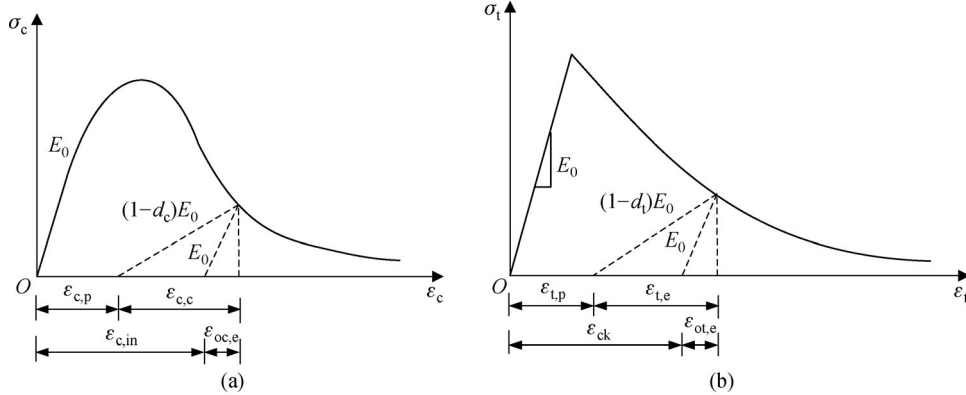


Fig. 4 Damage plasticity model for concrete under uniaxial compression and tension. (a) Compression; (b) tension.

where  $f_t$  is concrete tensile strength determined by the measured cube strength in accordance with Chinese code [57];  $\epsilon_t$  is the concrete uniaxial tensile strain;  $\sigma_t$  is concrete uniaxial tensile stress when concrete strain is  $\epsilon_t$ ;  $\epsilon_{t0}$  is the corresponding strain of concrete tensile strength and was taken as  $f_t/E_0$ ; and  $\alpha_t$  is a coefficient, taken as 2.81 in this study, to determine the descending portion of concrete stress-strain curve under tension.

As for concrete tension and compression damage parameters, extensive research has been conducted to investigate their values [61–63]. However, none of these methods has been exclusively recognized due to the complexity of concrete material. In this study, the damage parameters under compression and tension,  $d_c$  and  $d_t$ , were calculated using Eqs. (3)–(4).

$$d_c = 1 - \frac{\sigma_c}{E_0(\epsilon_c - \beta\epsilon_{c,in})}, \quad (3)$$

$$d_t = 1 - \frac{\sigma_t}{E_0(\epsilon_t - \lambda\epsilon_{t,in})}, \quad (4)$$

where  $\epsilon_c$  and  $\epsilon_t$  are concrete uniaxial compressive and tensile strains;  $\sigma_c$  and  $\sigma_t$  are the corresponding stresses when concrete strains are  $\epsilon_c$  and  $\epsilon_t$ , respectively;  $E_0$  is the Young’s modulus of concrete;  $\beta$  and  $\lambda$  are coefficients taken as 0.1 and 0.3, respectively, in this study;  $\epsilon_{c,in}$  and  $\epsilon_{t,in}$  are inelastic compressive strain and tensile strain under tension, given as follows:

$$\epsilon_{c,in} = \epsilon_c - \frac{\sigma_c}{E_0}, \quad (5)$$

$$\epsilon_{t,in} = \epsilon_t - \frac{\sigma_t}{E_0}. \quad (6)$$

### 3.4 Convergence study

A convergence study was conducted to determine suitable mesh sizes for concrete and reinforcement for the interior

beam-to-column joint. Taking SP1 as a case, the influences of mesh sizes of concrete and reinforcement in beam and column on load-displacement curves are shown in Fig. 5. It should be noted that all the FE models in the current study are full-scale three-dimension ones. The mesh sensitivity study shows that the mesh sizes of 50 mm are suitable, which can give accurate predictions of structural behaviors of the interior beam-to-column joint with reasonable computational costs.

### 3.5 Concrete damage parameters

Nonlinear behavior of concrete was considered by introducing tensile and compressive damage parameters into CDP model in ABAQUS. The values of the damage parameters have a significant influence on the simulation results of the behavior of the joints. Therefore, the influences of tensile and compressive damage parameters were studied in this section. Taking SP2 as an example, Fig. 6 presents the comparison of load-displacement curves of FE modeling results with experimental test data under four cases, i.e., no damage considered, only considering tensile damage, only considering compressive damage, and considering both tensile and compressive damage. It can be seen from Fig. 6 that the compressive damage parameter has a crucial influence on the ultimate capacity of the joint. Shayanfar and Akbarzadeh [64] also realized the importance of considering nonlinear behavior of concrete, reaching the conclusion that ignore nonlinearities in the joint core might crucially affect seismic performance of RC structures. For the case only compressive damage considered and neglecting tensile damage, the stiffness (slope) after cracking is obviously bias from the experimental result. However, after the yielding of longitudinal reinforcement, as the load approaching the ultimate state, the load capacity of FE model is close to the experimental result. Thus, if only considering the load capacity, the influence of tensile damage parameter can be neglected. On the other hand, the FE model considering

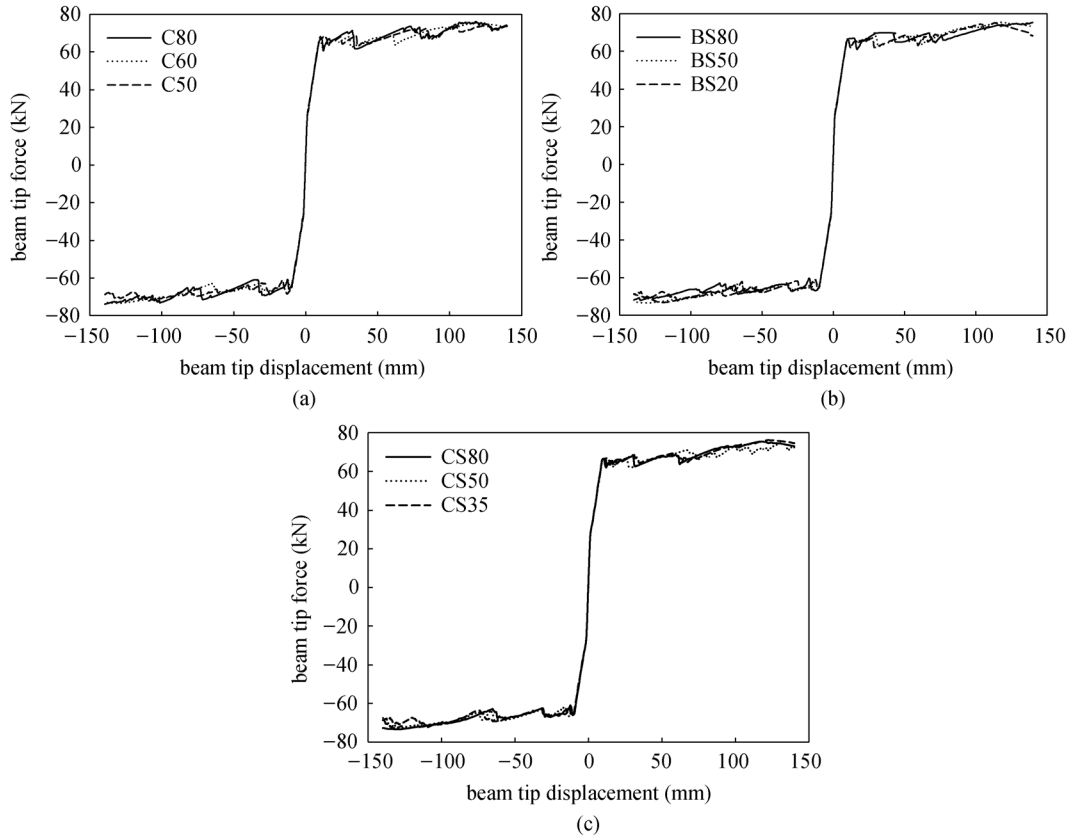


Fig. 5 The influence of mesh sizes on the load-displacement curves. (a) Concrete; (b) reinforcement in beam; (c) reinforcement in column.

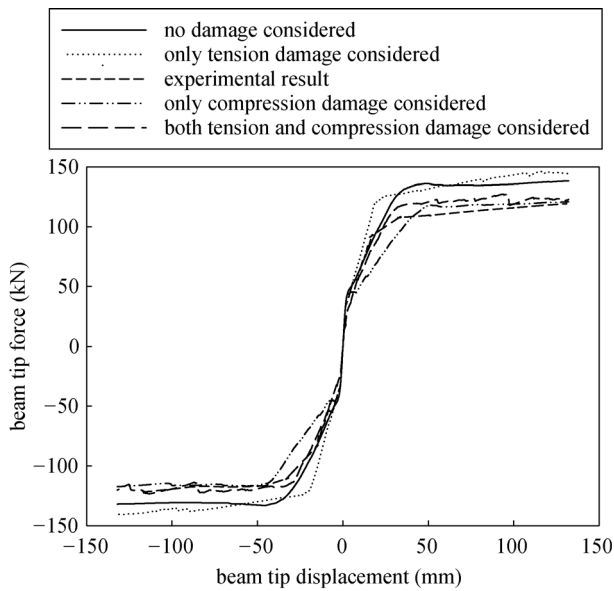


Fig. 6 The influence of concrete damage parameters on the load-displacement curves.

both compression and tension damage agrees well with the experimentally obtained curve. Therefore, to fully simulate the structural response of the RC joint, both tensile and

compressive damage parameters are incorporated in the FE models for concrete in the subsequent FE simulations.

### 3.6 FE models validation

To validate the FE models, the load-displacement curve of the beam tip (beam tip denoted as the point where vertical load was applied on beam element of the joint, as shown in Fig. 2), failure modes and tensile strains of the longitudinal reinforcement in beam element in joint adjacent region (the locations of strain gauges are shown in Fig. 1) measured in experimental tests were compared with those predicted by FE models.

Figure 7 shows the comparison of the load-displacement curves at the beam tip obtained from experiments and FE results. It could be seen that the FE models can replicate the load-displacement curves with a fair accuracy. On the other hand, failure modes of FE models and experimental tests for three specimens are shown in Fig. 8, in which PEMAG is the concrete plastic strain when the beam load reaches the peak and PEEQ is the accumulated equivalent plastic strain indicating the material yields when it is greater than zero. It could be seen from PEMAG nephograms that all three FE models experienced beam end flexural failure, which were in consistence with experimental results. According to the existing knowledge,

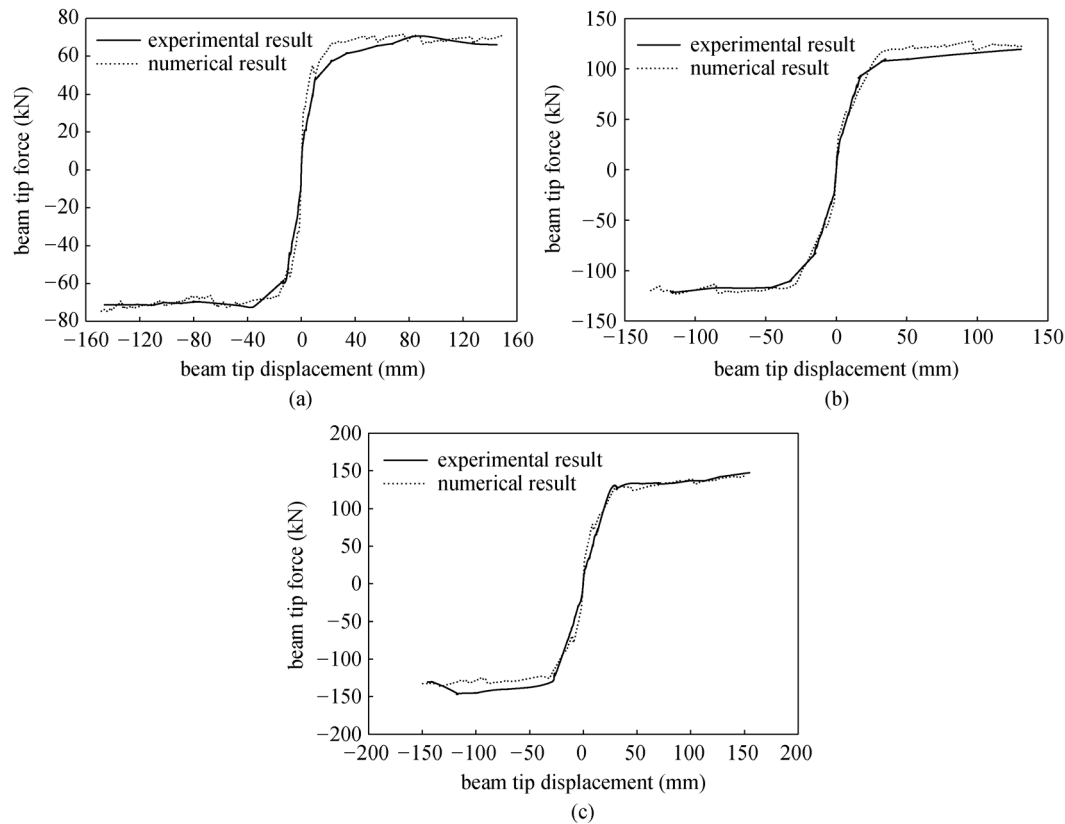


**Fig. 7** The comparison of load-displacement curves between FE models and experimental results. (a) SP1; (b) SP2; (c) SP3.

the shear stress level in joint core increases with the shear compression ratio [65–67]. Thus, SP3, having the largest shear compression ratio (0.32), reaches the most significant PEEQ. Although the PEEQ magnitude of SP1 with the smallest shear compression ratio of 0.12 is slightly larger than that of SP2, if only consider the joint core area, however, the PEEQ for SP2 with a larger shear compression ratio (0.27) is more significant than SP1 in term of area and extent. This can be reflected by more diagonal cracks in the joint core for SP2 as shown in Fig. 8. PEEQ for SP1 mainly occurred in the beam end areas, whereas for SP2 and SP3 the joint core experience more obvious PEEQ, which are consistent with the cracking modes shown in Fig. 8. In general, phenomena above were in accordance with experimental results so that FE outcomes were in good match with experimental results regarding to the failure mode.

The comparison of the tensile strain in the beam end tensile reinforcement in joint adjacent regions (see Fig. 1 for the location of strain gauge) between FE models and experiments is presented in Fig. 9. The FE models appeared to be slightly un-conservative compared to the experimental result. The maximum relative error is within 13.5% while the average relative error is within 10%, indicating FE simulations produced acceptable results with regards to the reinforcement strain.

It is inevitable that minor discrepancies existed between FE models and experimental tests due to a few assumptions in the FE models, e.g., the bond slip between reinforcement and concrete as well as the boundary conditions. However, the FE models used in the current work could produce acceptable results regarding to the load-displacement curves at beam tip, failure modes at joint core rejoin and tensile strain in the beam end tensile reinforcement in joint adjacent regions.

The evaluation of how the uncertain input parameters influence a specific uncertain output is significant to demonstrate the reproducibility of FE results. To solve this tough and easily overlooked problem, Rabczuk and his colleagues have done some valuable work. Hamdia et al. [28] developed a methodology for stochastic modeling of the fracture in polymer/particle nanocomposites. Vu-Bac et al. [29] put forward a framework that presents sequential steps consisting of generating random sample data by Latin Hypercube Sampling (LHS), transforming an arbitrary distributions into a multivariate normal distribution, approximating the observed data via surrogate models and estimating the sensitivity indices for the model with correlated parameters. However, since the current research focused on the mechanism investigation of RC beam column joint, a simplified conventional deterministic analysis is used to estimate the global responses of a

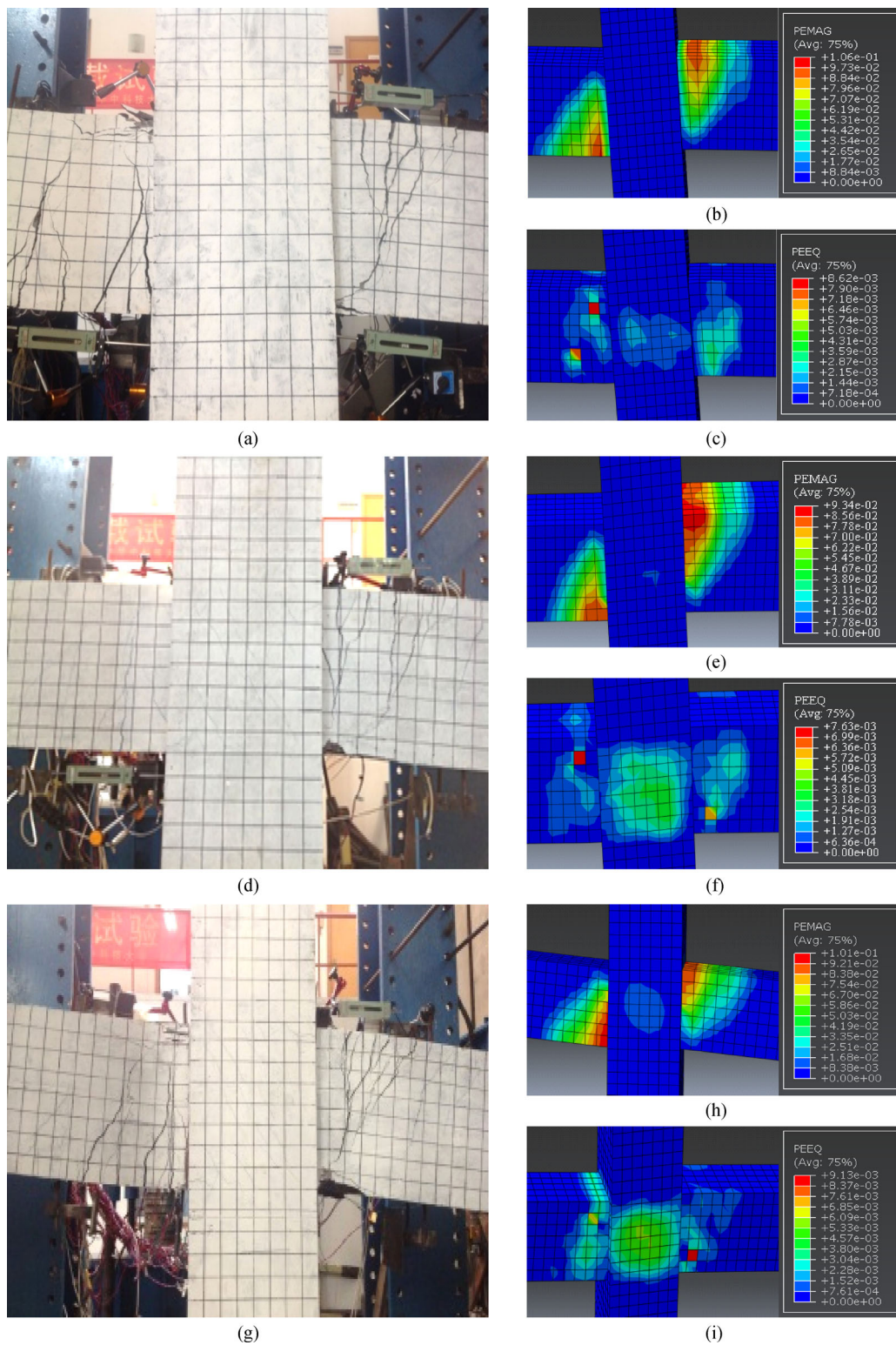


**Fig. 8** The comparison of failure modes between FE models and experimental results. (a) SP1: test; (b) SP1: PEMAG; (c) SP1: PEEQ; (d) SP2: test; (e) SP3: PEMAG; (f) SP3: PEEQ; (g) SP3: test; (h) SP3: PEMAG; (i) SP3: PEEQ.

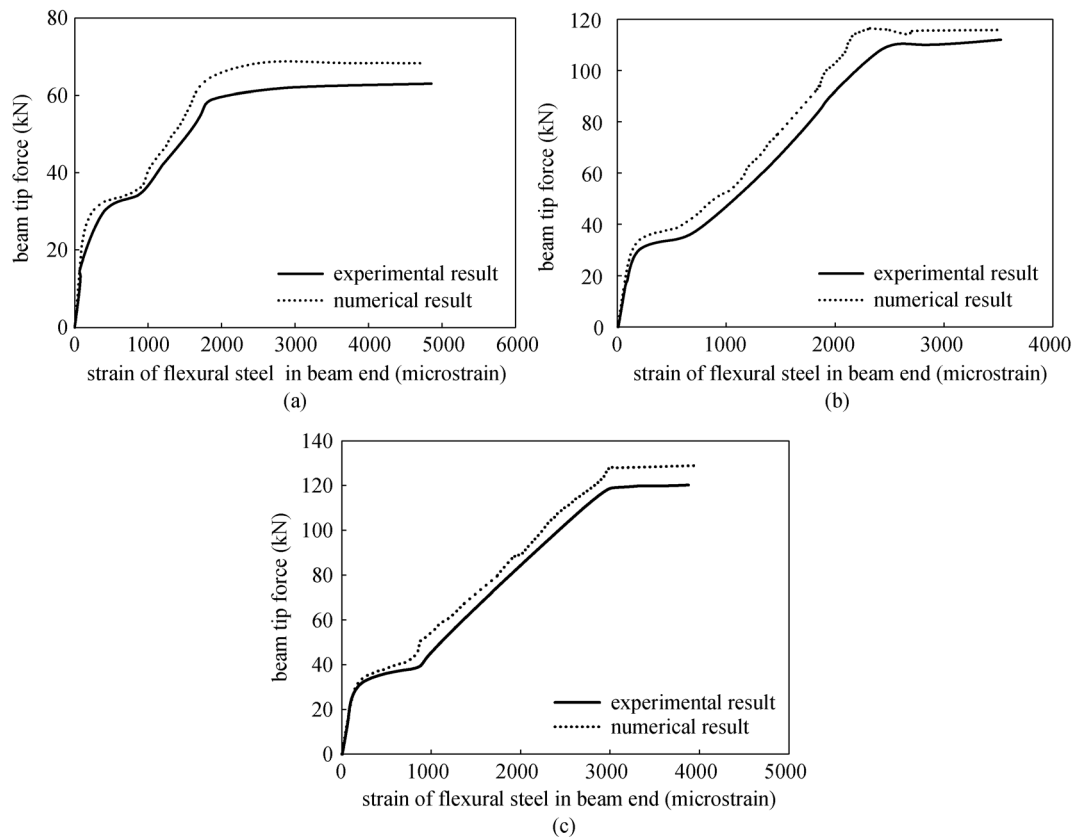


Fig. 9 The comparison of steel bar strain between FE models and experimental results. (a) SP1; (b) SP2; (c) SP3.

structure because a small variability exists in such levels [27].

#### 4 Influence of joint hoop reinforcement ratio on joint behavior

Difference regarding to RC beam-column joint design among different countries is mainly reflected by requirement of joint core hoop reinforcement ratio. However, consensus has been reached that shear failure should not be occurred before beam end longitudinal reinforcement yielding to ensure sufficient bearing capacity and ductility, since shear failure always occurs in brittle manner with small deflection. Therefore, a certain number of stirrups must be provided in the joint core to satisfy the requirement of minimum joint hoop reinforcement ratio. Influences of joint hoop reinforcement ratio on responses of RC beam-column joint would be investigated in this section.

Three groups of FE models under different shear-compression ratios and joint hoop reinforcement ratios were established. Details of the FE models are as summarized in Table 3. The concrete cover is set as 25 mm. Stirrups in joint core are placed symmetrically along central axial surface as shown in Fig. 10. JT0 represents

stirrup located in the central axial surface, while JT*i*B and JT*i*T ( $i = 1, 2, \text{ or } 3$ ) denote stirrups arranged symmetrically about central axial surface with B and T indicating bottom and top directions, respectively. Considering the randomness of intersecting points between diagonal cracks and stirrups in the joint core area, the weighted average strain of each stirrup element in a stirrup leg parallel to beam length (P-direction) was denoted as JT0-P strain value, while average strain of another two stirrup legs vertical to beam length (V-direction) was chosen as JT0-V strain value.

##### 4.1 Effect of joint hoop reinforcement ratio on stirrup strain against column end axial compressive load

Variation of average stirrup strain in joint core under the process of applying column end axial compressive load (without load applied on beam tip) is shown in Fig. 11. An interesting phenomenon could be seen from the figure that stirrup strain in joint core was in proportion to column end axial compressive load with the maximum strain occurred in stirrup located in the central of the joint. The further from the central region, the smaller stirrup strain could be. Strain values of stirrups that are located vertically symmetric were almost the same in joint core, indicating a relatively even expansion of concrete in the limited

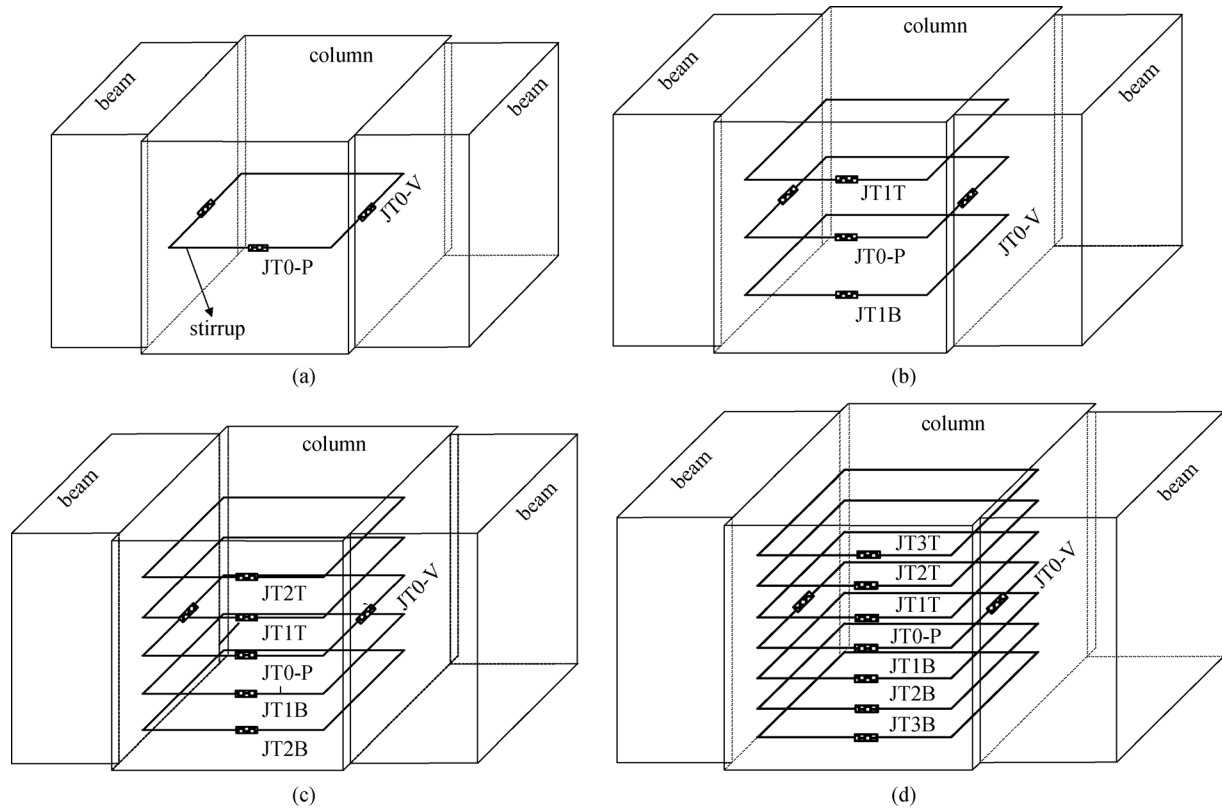


**Fig. 10** The joint core transverse reinforcement ratio ( $\rho_{sv,j}$ ) and the stirrup numbering. (a)  $\rho_{sv,j}$  at 0.17%; (b)  $\rho_{sv,j}$  at 0.51%; (c)  $\rho_{sv,j}$  at 0.86%; (d)  $\rho_{sv,j}$  at 1.20%.

**Table 3** Summary of FE models for parametric study

group	ID of FE model	steel bar kind	beam		column		stirrup in joint core		$\nu$	$\lambda$
			cross section (mm)	tension steel	cross section (mm)	longitudinal steel	number	$\rho_{sv,j}$		
1	NS1	HRB335	300×400	2Φ20	400×400	12Φ20	1Φ10	0.17	0.3	0.12
	NS2	HRB335	300×400	2Φ20	400×400	12Φ20	3Φ10	0.51		
	NS3	HRB335	300×400	2Φ20	400×400	12Φ20	5Φ10	0.86		
	NS4	HRB335	300×400	2Φ20	400×400	12Φ20	7Φ10	1.20		
2	NS5	HRB500E	300×400	3Φ20	400×400	12Φ20	1Φ10	0.17	0.3	0.27
	NS6	HRB500E	300×400	3Φ20	400×400	12Φ20	3Φ10	0.51		
	NS7	HRB500E	300×400	3Φ20	400×400	12Φ20	5Φ10	0.86		
	NS8	HRB500E	300×400	3Φ20	400×400	12Φ20	7Φ10	1.20		
3	NS9	HRB600	300×400	3Φ20	400×400	12Φ20	1Φ10	0.17	0.3	0.32
	NS10	HRB600	300×400	3Φ20	400×400	12Φ20	3Φ10	0.51		
	NS11	HRB600	300×400	3Φ20	400×400	12Φ20	5Φ10	0.86		
	NS12	HRB600	300×400	3Φ20	400×400	12Φ20	7Φ10	1.20		

Note:  $\rho_{sv,j}$  = Volume reinforcement ratio of joint core;  $\nu$  = axial-compression ratio;  $\lambda$  = shear-compression ratio.

length within joint core area. Furthermore, it could be seen that, as joint hoop reinforcement ratio increases, strain in stirrup decreased and strain distribution became more uniform, which agrees well with the existing experimental results [68–70]. The primary reason for this phenomenon

could be that, due to more even confinement provided by closely spaced stirrups, the dilation of joint core concrete is well restrained resulting in a more even distribution of lateral strain in concrete. In addition, with the increase of joint hoop reinforcement ratio, the restraining effect of

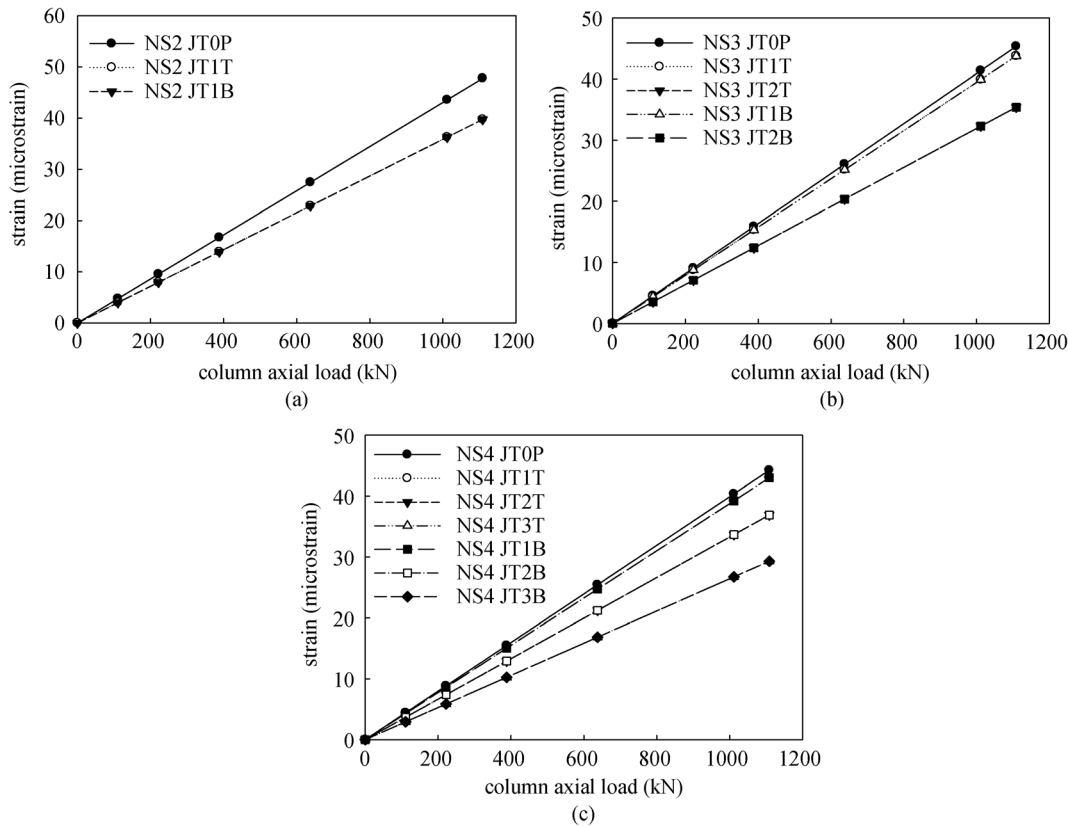


**Fig. 11** The relationship between the stirrup strain in joint core and axial force applied on column end. (a)  $\rho_{svj}$  at 0.51% for NS2; (b)  $\rho_{svj}$  at 0.86% for NS2; (c)  $\rho_{svj}$  at 1.20% for NS2.

stirrups on joint concrete was enhanced, and the resulted strain value in each stirrup was reduced.

#### 4.2 Effect of joint hoop reinforcement ratio on cracking and yielding load of beam element

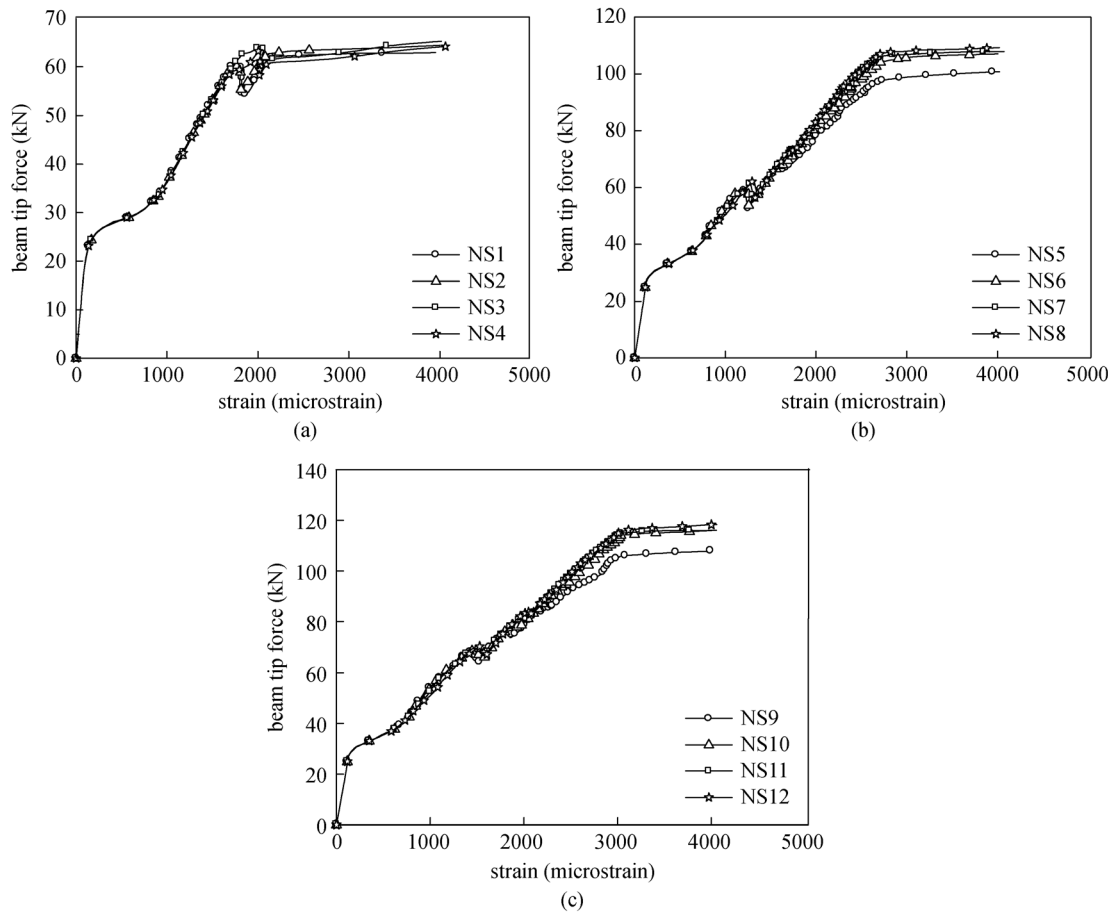
Cracking load of the RC beam-column joint is defined as the beam tip transverse load (refer to Fig. 2) causing the initial flexural crack of beam end near joint area. Yielding load of RC beam-column joint in this work is defined as the load applied in beam tip causing the yield of tensile reinforcement of beam element near the joint (the location of strain studied is shown in Fig. 2), and the corresponding beam tip displacement is denoted as yield displacement. Influences of joint hoop reinforcement ratio on cracking and yielding loads of beam element under different shear-compression ratios are shown in Fig. 12.

Figure 12 shows that the cracking load for all the cases is around 25 kN even though the joint core hoop reinforcement ratio increased from 0.17% to 1.2%, indicating the joint core hoop reinforcement ratio exerted little influence on cracking load of beam component regardless of the value of shear-compression ratios (0.12, 0.27, and 0.32). On the other hand, it could be found that, under medium (0.27) and large shear-compression ratio (0.32), the yielding load of beam element increases with the increase

of joint core hoop reinforcement ratio, but the increment could be very small when joint core hoop reinforcement ratio was larger than 0.51%. The effect of joint hoop reinforcement ratio showed little influence on the yielding load of beam component under small shear-compression ratio (0.12). In addition, it could be noted in the figure that all the curves experienced a minor fluctuation in trend: they descended first (at around 60 kN) and ascended shortly when longitudinal steel bar strain near the joint core (location of strain refer to Fig. 2) reached around 1500 microstrain. This can be attributed to the fact that beam longitudinal reinforcement throughout the joint core experienced stress redistribution due to the formation of new cracks in both beam component and joint core.

#### 4.3 Effect of joint hoop reinforcement ratio on yielding displacement of beam element

The effect of joint core hoop reinforcement ratio on the yielding displacement (the location of strain studied is shown in Fig. 2) of beam under different shear-compression ratios are shown in Fig. 13. For Groups 1 and 2, it is found that beam end yielding displacement decreased with the increase of joint core hoop reinforcement ratio. However, this trend became rather insignificant when the ratio reached a certain value. However, For RC beam-



**Fig. 12** Effect of joint core transverse reinforcement ratio on cracking and yielding load of beam element. (a) Group 1; (b) group 2; (c) group 3.

column joint with higher shear compression ratio (for example SP3 with shear compression ratio of 0.32), more shear stress is transferred to the joint core through strut-and-tie and truss mechanisms [65–67]. As a result, larger shear deformation and more shear cracks are expected to occur in the joint core (Fig. 8), which is also consistent with the findings obtained by Fu et al. [65,66] as well as Zhang and Wang [67]. For Group 3, on the one hand, too much hoop reinforcement in joint core contributes little to restrain the deformation of joint core. On the other hand, larger shear compression ratio (0.32) increased the shear deformation of joint core. Thus, under these two opposite deformation mechanisms, the effect of joint core hoop reinforcement is not clear. Further research on the combined effect of joint core hoop reinforcement ratio and shear compression ratio is need to clarify their effects on the yielding deformation of RC joint.

#### 4.4 Effect of joint hoop reinforcement ratio on cracking load of joint core

The influence of joint core hoop reinforcement ratio on cracking load of joint core under different shear-compress-

ion ratio is shown in Fig. 14. The strain values presented in Fig. 14 is the average strain value of stirrup leg JT0-P as illustrated in Fig. 10, which is assumed to be intersected by diagonal cracks in joint core. The cracking load of the joint core is represented as the sharp increase of strains in stirrups. It could be clearly seen that the increase of hoop reinforcement ratio in joint core delayed the cracking of joint core to some extent and thus slightly improved cracking load. But the increment became very insignificant after joint core hoop reinforcement ratio reached a certain degree. Owing to the increase of joint core hoop reinforcement ratio, the restrain effect on joint core concrete was enhanced, and a more uniform stress distribution of concrete was generated so that the cracking of joint core concrete could be postponed and crack load could be slightly improved.

To explain the stirrup strain variation, the mechanism of shear transfer in the joint core need to be reviewed. It is commonly accepted that RC beam-column joints resist shear by the strut and truss mechanisms as first pointed out by Paulay et al. [2]. The strut mechanism accounts for the contribution of the concrete, whereas the truss mechanism represents the contribution of stirrups. The initial value of

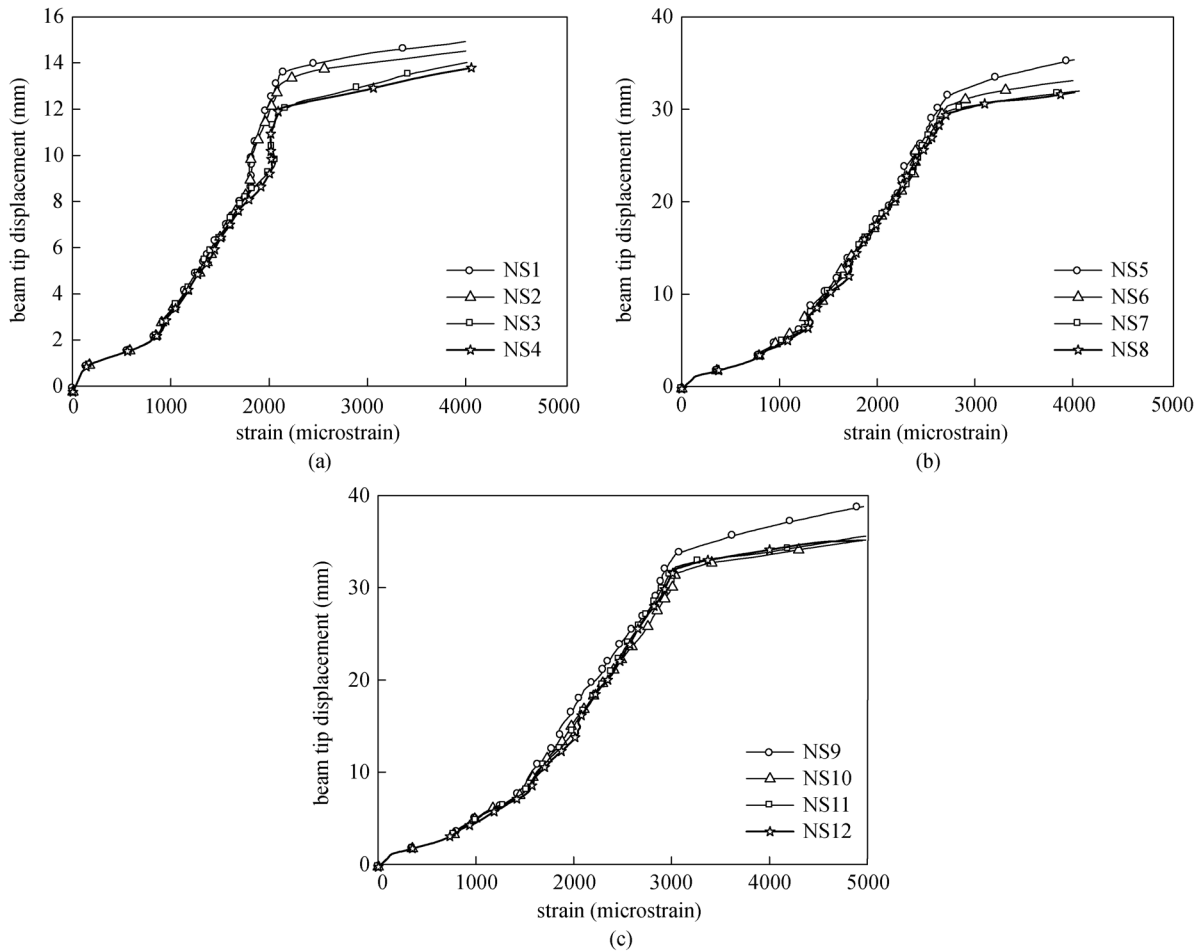


**Fig. 13** Effect of joint core transverse reinforcement ratio on yielding displacement of beam element. (a) Group 1; (b) group 2; (c) group 3.

strain in stirrup is due to the column axial load. At the beginning of loading the beam, the concrete in the joint core suffers to limited stress level, and the stress in the joint is mainly transferred by strut mechanism. Thus, the stirrup strain seems unchanged. As the increase of load, the horizontal component of compressive force in the diagonal strut becomes more and more significant, which makes the stirrup in the joint core under a compression state. Thus the stirrup strain decrease. Once the cracking of the joint core occurs, truss mechanism plays an important role. The strain of stirrup crossing the diagonal crack increase sharply. Similar results have been obtained by Haach et al. [20].

#### 4.5 Effect of joint hoop reinforcement ratio on stirrup strain vs. $\Delta/\Delta_y$ curves

A comparison of average stirrup strain in P- and V-direction (the directions refer to Fig. 10(a)) under different shear-compression ratios is shown in Fig. 15, in which  $\Delta$  and  $\Delta_y$  represent beam displacement under loading point and the displacement causing the yield of tension steel at

the end of beam (location of strain used refer to Fig. 2), respectively. Due to the randomness of distribution of diagonal cracks in joint core, five evenly-spaced points covering the whole length of stirrup legs in P- and V-direction were used to obtain the corresponding average strains. It is observed that the passive constrain forces sustained by stirrups in P- and V-directions were not necessarily equal in magnitude, which could be clearly seen from Fig. 15. Strains of stirrups in both directions were close to each other under medium and high shear-compression ratios (e.g., 0.27 and 0.32) when the displacement reached between 2 to 3 times of the  $\Delta_y$ .

It could be seen that stirrup strain in P-direction was always larger than that in V-direction, which is attributed to the fact the diagonal cracks are mainly intersected with stirrups in P-direction, as experimentally and numerically illustrated in Fig. 8. After diagonal cracking in joint core, strut-and-tie mechanism was triggered in the joint to transfer shear, resulting in larger sustained strains in stirrup legs in P-direction. According to constitutive characteristics of concrete, as the increase of the diagonal compressive strain, expansion in the other two orthogonal

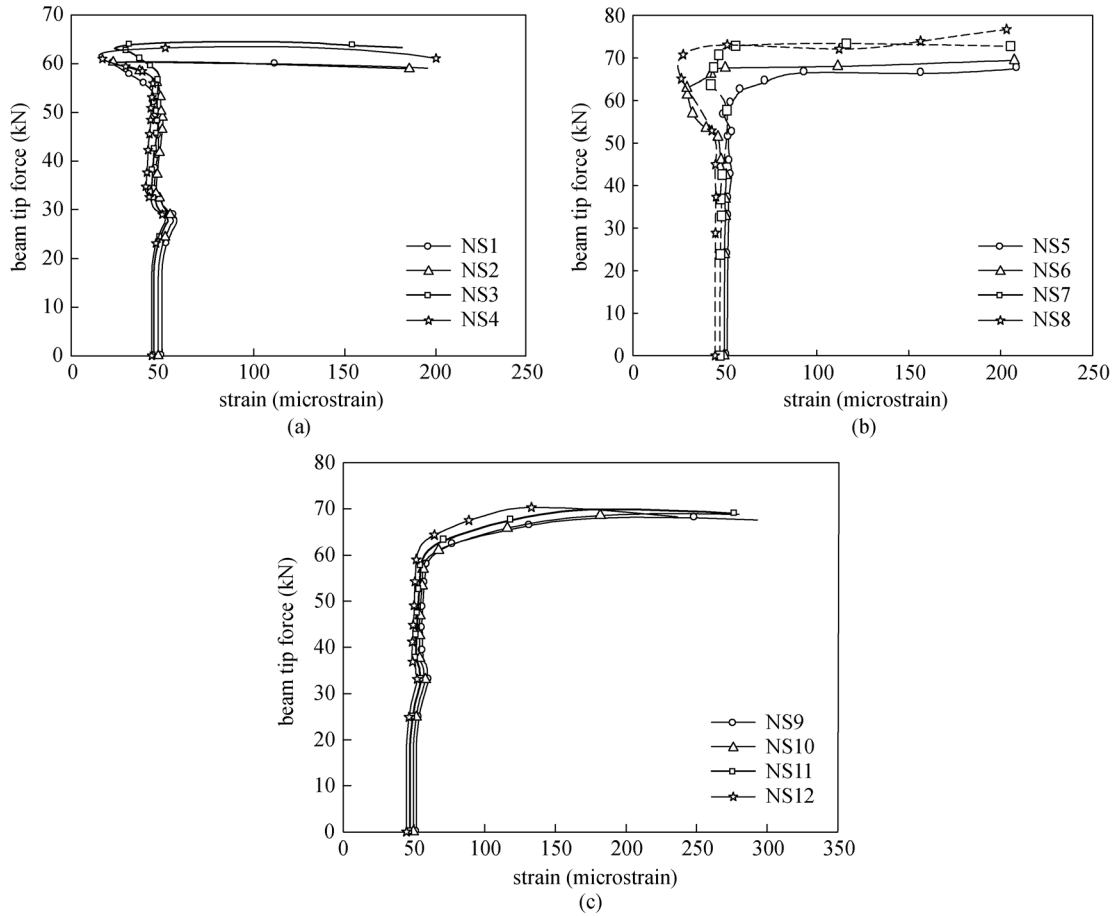


Fig. 14 Effect of joint core transverse reinforcement ratio on cracking load of joint core. (a) Group 1; (b) group 2; (c) group 3.

directions transverse to principal compression was increasing accordingly. Stirrup legs in V-direction did not resist shear directly, instead, the strains of which were mainly caused by lateral expansion of diagonal compressive concrete struts generated by truss mechanism and the passive constrain effect preventing outward buckling of column longitudinal reinforcement due to axial load.

Another phenomenon is that with the increase of joint core hoop reinforcement ratio, stirrup strains in both V- and P-directions decreased, and the differences of strain between adjacent stirrups were descending, too. This indicates that, at larger hoop reinforcement ratio, the strains in one stirrup is more uniform due to more even dilation of concrete and that shear cracks in joint core concrete are well restrained, which is consistent with the experimental finding obtained by Wu and Hu [71] and Hu and Wu [72,73].

It could be concluded from above analysis that the restrain mechanism within the joint core existed in addition to strut-and-tie mechanism. Arranging a certain number of horizontal stirrups could not only improve the yielding load of beam element, reduce the yielding displacement and increase the joint ductility, but also play a significant role in strengthening the restraining effect on joint core

concrete. Additionally, those stirrups can also resist certain part of shear stress in joint core, preclude outward buckling of longitudinal reinforcement, enhance the stress distribution as well as enable stress redistribution and increase joint seismic resistance capacity. However, excessive amount of stirrups is unnecessary since they are not fully engaged in enhancing joint behavior.

## 5 Influence of axial load ratio

Axial load ratio is a significant factor that influences the mechanical behavior of RC beam-column joint [9,20,23,39]. However, consensus has not yet been reached in research community for the understanding of this problem. To study the influence of axial load ratio, FE models NS1, NS5, and NS9 (Table 3) under axial load ratios of 0.1, 0.3, 0.5, 0.7, and 0.9 were investigated.

### 5.1 Effect of axial load ratio on reinforcement strains (without beam tip force)

The influence of axial load ratio on beam longitudinal reinforcement strain in joint adjacent regions is shown in

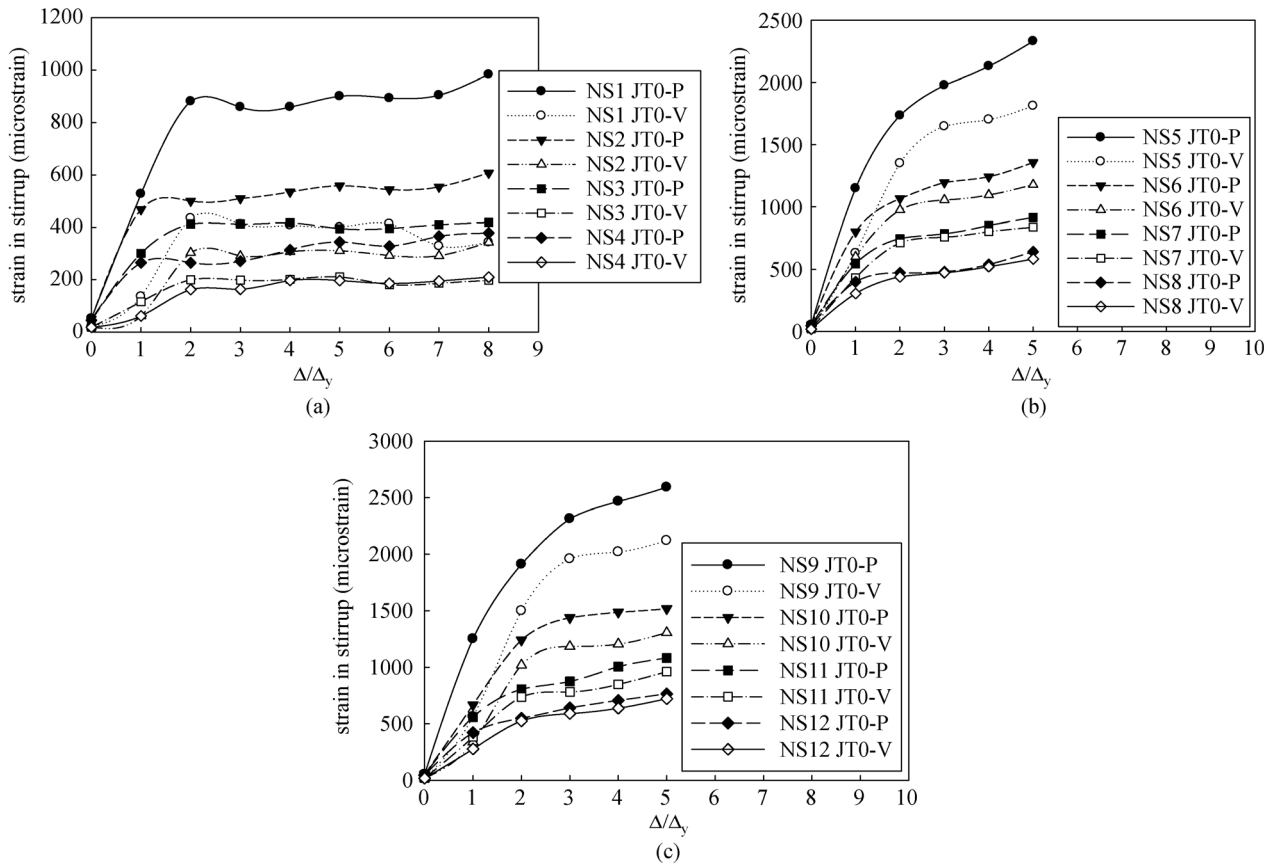


Fig. 15 Effect of joint core transverse reinforcement ratio on stirrup strain vs.  $\Delta/\Delta_y$  curves. (a) Group 1; (b) group 2; (c) group 3.

Figs. 16 and 17. The number and location of rebar elements studied are illustrated in Fig. 18. It could be seen that beam end reinforcement in joint adjacent regions experienced tensile strain in the process of application of column end axial compressive load. It can be also observed in that the higher axial load ratio was, the larger tensile strain would be. The strains increased proportionally under low or medium axial load ratios. However, under high axial load ratio, tensile strain increased sharply when the axial load was approaching the maximum value. Figure 17 shows the relationship between the strain of longitudinal reinforcement elements near the joint core and axial load ratio. It can be found that the strains of elements 1, 2, 3, and 4 coincided very well. Three mechanisms can be found behind this phenomenon. First, as the increase of column axial load, the slight axial compression deformation in the joint core causes a tensile strain in beam longitudinal reinforcement near column face; the second is the Poisson's ratio effect; and the third is lateral expanded deformation of concrete transfers a portion of tensile force to steel reinforcement due to the bond.

5.2 Effect of axial load ratio on cracking and yielding load of beam element

The effects of the axial load ratio on the cracking load and

yielding load of beam element are shown in Fig. 19. The location of strain presented in Fig. 19 is illustrated in Fig. 2. The definition of cracking load and yielding load of beam element are stated previously. It is observed that, under smaller values (from 0.1 to 0.7), the axial load ratio showed little influence on beam end cracking load. However, the beam end cracking load declined obviously under higher axial load ratio of 0.9.

For NS1, under small shear-compression ratio at 0.12, the yielding load of beam element increased first as the axial load ratio increased from 0.1 to 0.5, while it decreased when the axial load ratio continued to increase from 0.7 to 0.9. However, for NS5 and NS9 with higher shear-compression ratio at 0.27 and 0.32, respectively, yielding load of beam component continued to increase as the axial load ratio increases but the increment is insignificant once the axial load ratio larger than 0.5. These observations show that the increase of the axial load ratio can enhance the joint capacity to some degree, which depends on the shear-compression ratio values.

5.3 Effect of axial load ratio on cracking and yielding displacement of beam element

Figure 20 shows the effect of the axial load ratio on the beam end cracking and yielding displacement. The

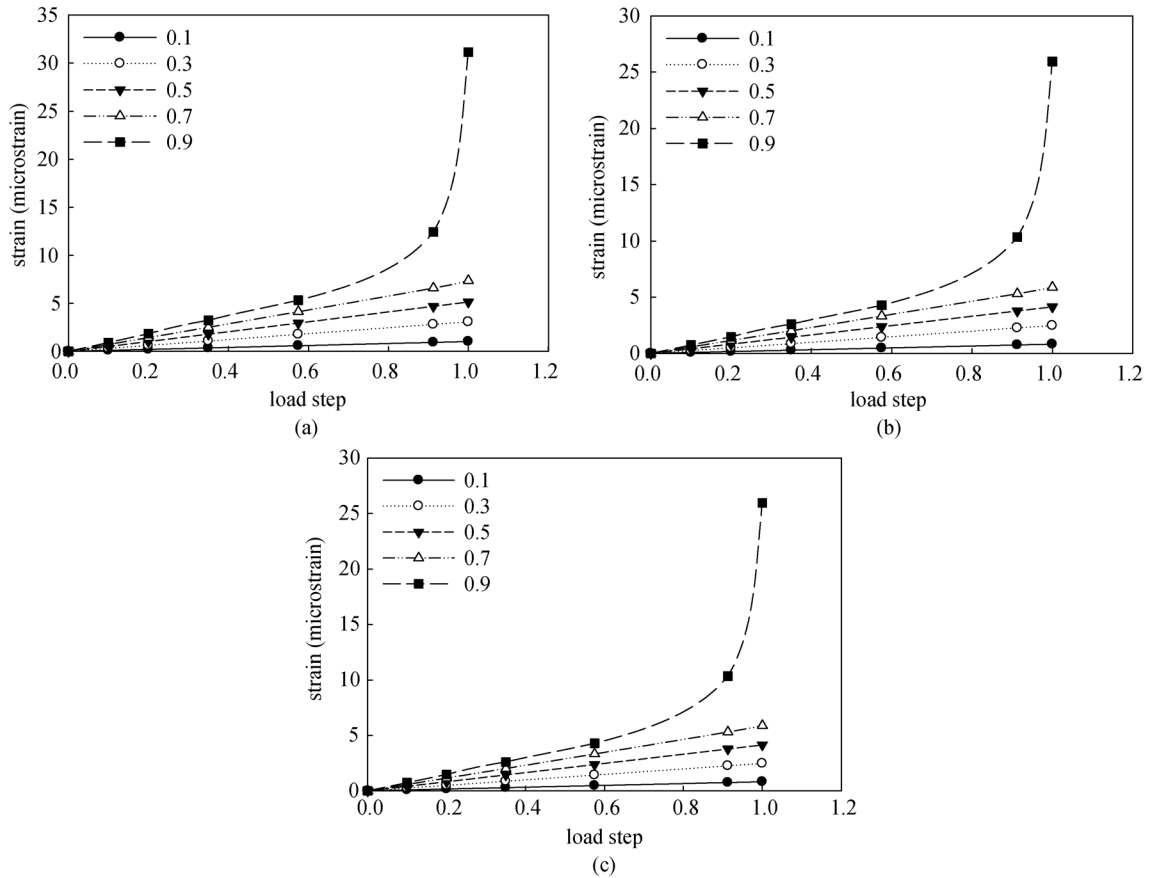


Fig. 16 The effect of applying the column end axial force on strain of steel element 3. (a) NS1; (b) NS5; (c) NS9.

location of strain presented in Fig. 20 is illustrated in Fig. 2. Generally, with the increase of the axial load ratio, the beam end yielding displacement decreased, but the decline was insignificant when the axial load ratio reached a certain value. This was due to the fact that the stiffness of joint core increased with the increase of the axial load ratio so that the shear deformation of joint was restrained to some extent, and thus the beam end yielding displacement declined accordingly. On the one hand, the axial compressive load can increase the flexural stiffness of the joint. The beneficial confinement effect from axial compressive load enables the columns being confined with limited flexural rotation, thus the lateral displacement contributed by column flexural and column fixed-end rotation was not significant, as experimental observed by Li and Leong [23]. In addition, the presence of the column axial compression enhances the strong column-weak beam behavior and moves the neutral axis toward reducing the tensile stress of the longitudinal column reinforcement, which directly reduces the curvature of column [9]. On the other hand, the axial compressive load restrains the crack width of diagonal cracks in the joint core, and thus reduces the shear deformation [6]. No obvious trend was observed for the cracking displacement under varying axial load ratios. The cracking of beam is mainly controlled by the

tensile strength of concrete. In addition, steel bars are activated to play a role only after the flexural cracking. As a result, the axial compression ratio has very little influence on the cracking displacement regardless of the shear compression ratio values.

5.4 Effect of axial load ratio on cracking load of joint core concrete

The influence of the axial load ratio on the cracking load of joint core is shown in Fig. 21. The cracking is characterized by the sharp increase of strain. The strain values presented in Fig. 21 is the average strain value of stirrup leg JT0-P as illustrated in Fig. 10, which is assumed to be intersected by diagonal cracks in joint core. It could be seen that the joint core crack load increased to some degree under low shear-compression ratio (0.12) when the axial load ratio increased from 0.1 to 0.7. But the axial load ratio slightly influenced the cracking load of joint core when the axial load ratio increased to a certain value, e.g., 0.9. Under medium and high axial load ratio (0.27 or 0.32), the cracking load of joint core increased gradually when the axial load ratio increased from 0.1 to 0.7. Nevertheless, the cracking load of joint core had a significant decline when the axial load ratio ranged from 0.7 to 0.9, which

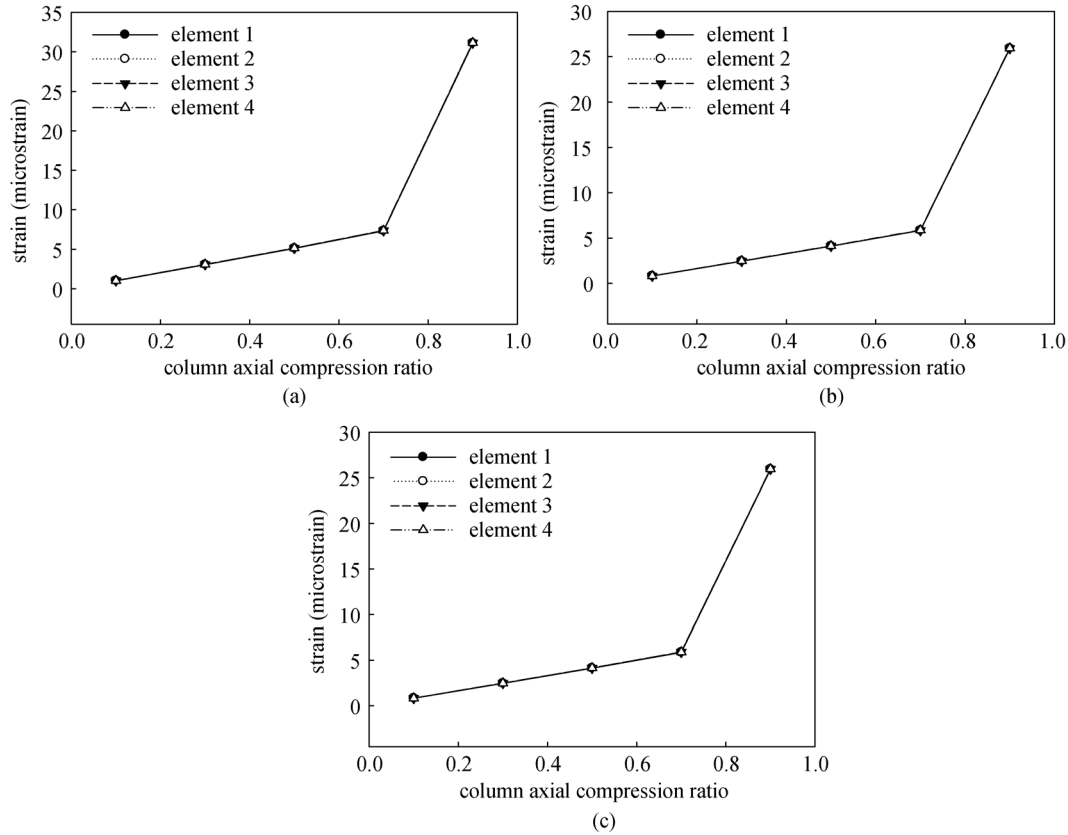


Fig. 17 The effect of compression axial ratio on strain of steel in beam near joint core. (a) NS1; (b) NS5; (c) NS9.

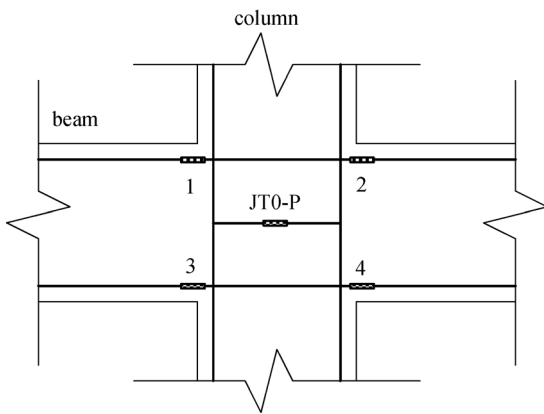


Fig. 18 Numbering and location of steel elements of longitudinal steel bars in beam element.

indicates that high axial load ratio had disadvantageous impacts on the joint core behavior, which agrees well with the finding obtained by Li and Leong [23].

## 6 Conclusions

In this paper, three-dimensional solid elements and CDP model are used to analyze the RC interior beam-column

joints under monotone antisymmetric loading by means of ABAQUS. The effects of tension and compression damage and mesh size on the load-displacement curve of the beam are studied. The influence of the axial compression ratio and the reinforcement ratio of the core region on the structural responses of the RC interior beam-column joints is presented, compared, and analyzed. The following conclusions are drawn:

1) For CDP model, the compression damage of concrete has a significant influence on the structural responses of RC interior beam-column joints. The capacity of the joint decreases with the increase of the concrete compression damage. Concrete tensile damage affects the post cracking stiffness of the joint, whereas its influence on the joint capacity is insignificant. It is suggested that both the compressive and tensile damage of concrete should be considered in FE model if the structural response of a joint during the whole load process need to be captured.

2) Under the same shear-compression ratio, the transverse reinforcement ratio in joint core exerts insignificant influence on the cracking load of beam end. Under shear-compression ratio of 0.12, the effect of transverse reinforcement ratio of joint core on the yielding load of beam end can be neglected. However, under medium (0.27) and high shear-compression (0.32) ratios, the yielding load increase with the increasing transverse

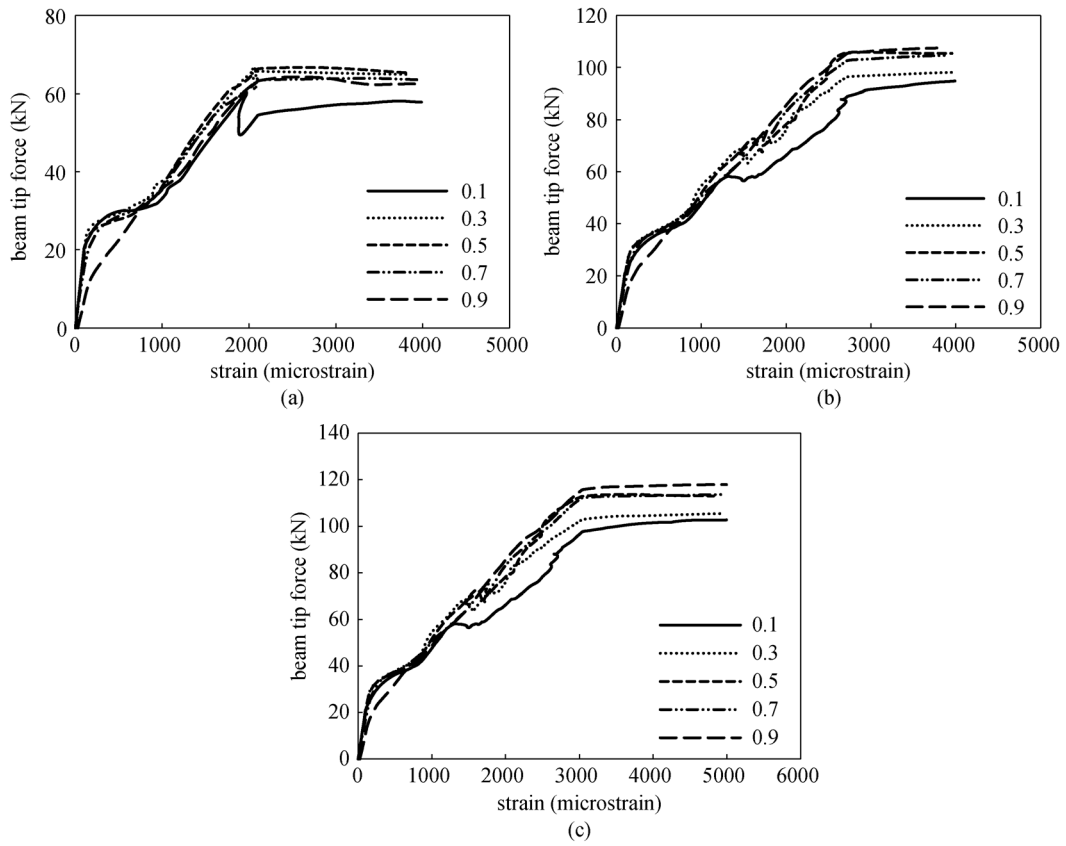


Fig. 19 Effect of axial load ratio on cracking and yielding load of beam element. (a) NS1; (b) NS5; (c) NS9.

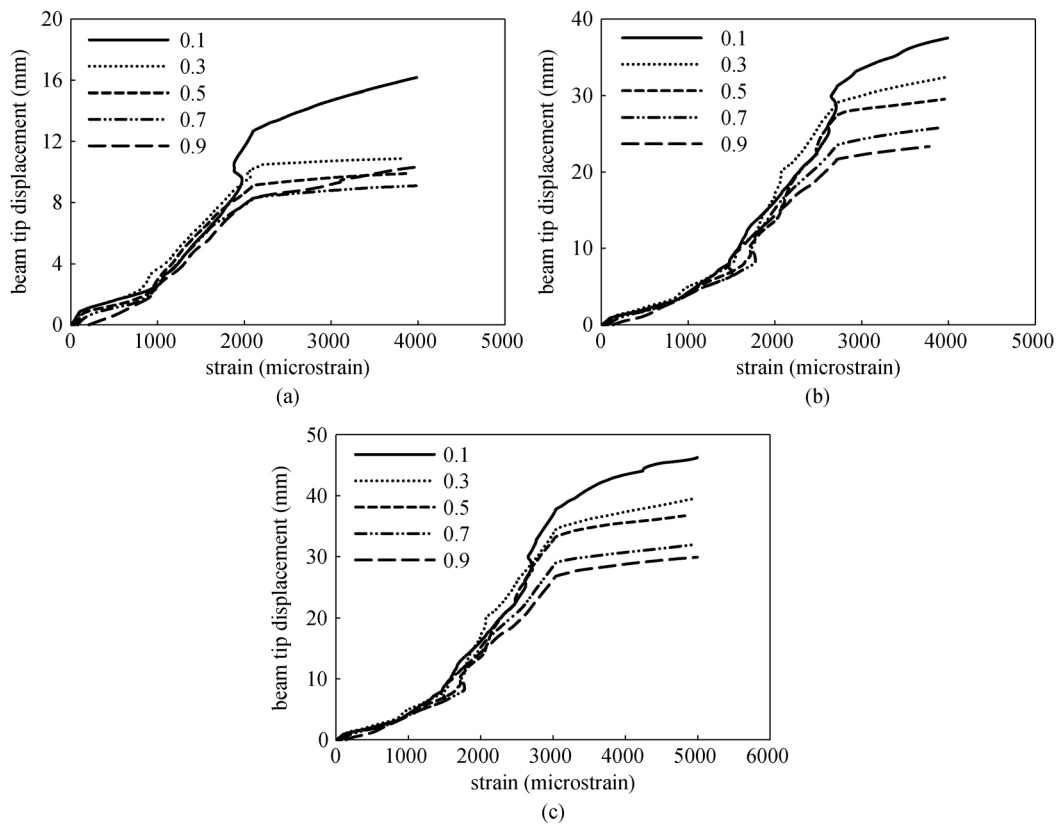


Fig. 20 Effect of axial load ratio on cracking and yielding displacement of beam element. (a) NS1; (b) NS5; (c) NS9.

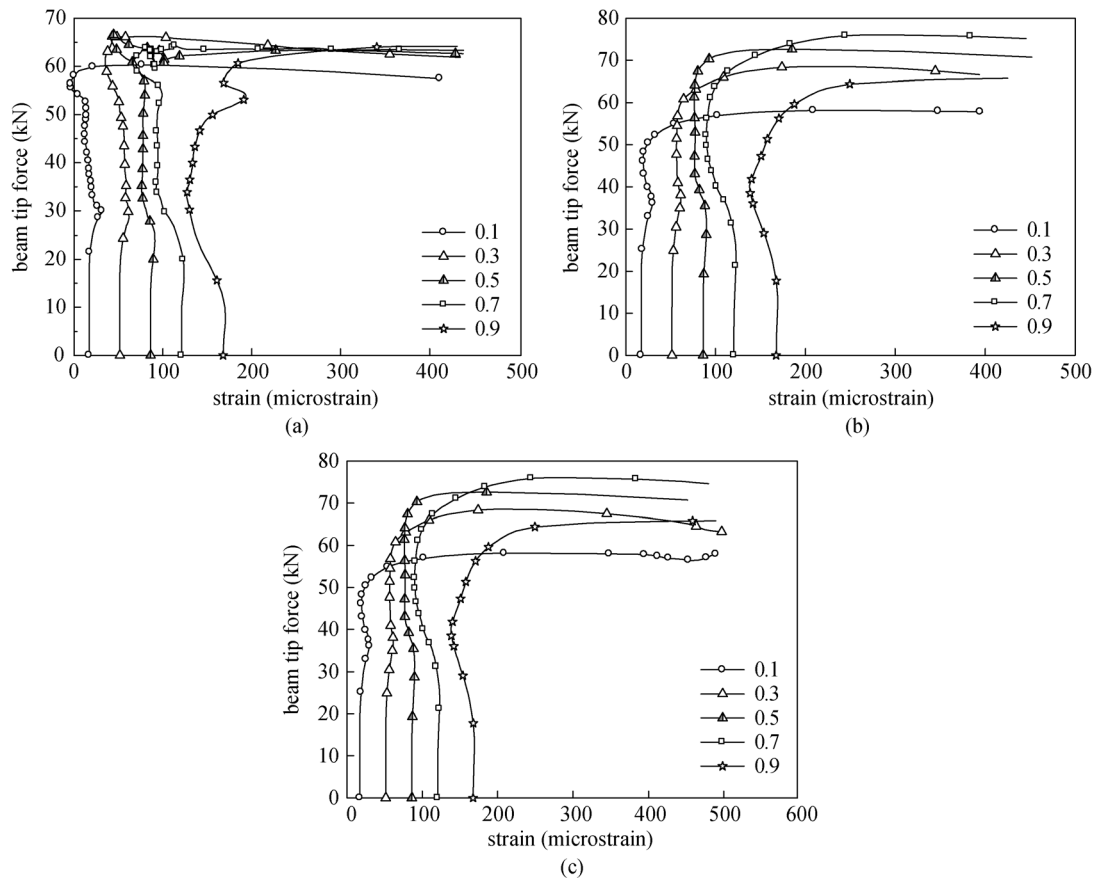


Fig. 21 Effect of axial load ratio on cracking load of joint core concrete. (a) NS1; (b) NS5; (c) NS9.

reinforcement ratio in joint core if the ratio is less than 0.51%. However, this positive effect becomes insignificant when the transverse reinforcement ratio of joint core is larger than 0.51%.

3) In addition to the presence of the truss mechanism, there is a constraint mechanism in the joint core area. A certain amount of horizontal stirrups can increase the yield load of beam end, increase the ductility of the joint, enhance the constraint effect on the concrete, transfer shear and prevent the outward buckling longitudinal reinforcement.

4) Under small and medium shear-compression ratios (0.12 and 0.27), the yielding displacement decreases with increasing joint hoop reinforcement ratio provided that the ratio is less than 0.86%. Further increase of the joint hoop reinforcement ratio exerts little influence on the yielding displacement of joint. Under a larger shear compression ratio (0.32), the effect of joint hoop reinforcement ratio on the yielding deflection can be neglected if the ratio is larger than 0.51%.

5) The effect of axial load ratio on yielding load of beam element is affected by shear compression ratio. Under a shear compression ratio of 0.12, the yielding load of beam increase with the increase of axial load ratio when the ratio is not greater than 0.3. Otherwise, if axial load ratio is

greater than 0.3, the yielding load of beam will not increase or even decrease with the axial load ratio. Under a higher shear compression ratio such as 0.27 or 0.32, yielding load of beam element is enhanced by increasing axial load ratio until a value of 0.5.

**Acknowledgements** The work described in this paper was supported by the National Key Research & Development Plan of China (No. 2016YFC0802002), and Key Interdiscipline Research Plan of Huazhong University of Science and Technology (No. 2016JCTD113).

## References

1. Park R, Paulay T. Behavior of reinforced concrete external beam-column joints under cyclic loading. In: Proceedings of the 5th World Conference on Earthquake Engineering. Rome, 1973, 772–781
2. Paulay T, Park R, Prestley M J N. Reinforced concrete beam-column joints under seismic actions. ACI Journal Proceedings, 1978, 75(11): 585–593
3. Ehsani M R, Wight J K. Exterior reinforced concrete beam-column connections subjected to earthquake type loading. ACI Journal Proceedings, 1985, 82(4): 492–499
4. Durrani A J, Wight J K. Behavior of interior beam-to-column connections under earthquake-type loading. ACI Journal Proceed-

- ings, 1985, 82(3): 343–349
5. MacGregor J G, Wight J K, Teng S, Irawan P. Reinforced concrete: Mechanics and design. Upper Saddle River, NJ: Prentice Hall, 1997
  6. Alaaee P, Li B. High-strength concrete exterior beam-column joints with high-yield strength steel reinforcements. *Journal of Structural Engineering*, 2017, 143(7): 04017038
  7. Alaaee P, Li B. High-strength concrete exterior beam-column joints with high-yield strength steel reinforcements. *Engineering Structures*, 2017, 145: 305–321
  8. Park S, Mosalam K M. Analytical model for predicting shear strength of unreinforced exterior beam-column joints. *ACI Structural Journal*, 2012, 109(2): 149–159
  9. Kim J, LaFave J M. Key influence parameters for the joint shear behaviour of reinforced concrete (RC) beam-column connections. *Engineering Structures*, 2007, 29(10): 2523–2539
  10. Sharma A, Eligehausen R, Reddy G R. A new model to simulate joint shear behavior of poorly detailed beam-column connections in RC structures under seismic loads, Part I: Exterior joints. *Engineering Structures*, 2011, 33(3): 1034–1051
  11. Standards New Zealand. Concrete Structures Standard: Part 1—The Design of Concrete Structure. NZS 3101, Standards New Zealand, Wellington, New Zealand, 2006
  12. ACI. Building Code Requirements for Structural Concrete. ACI 318-08, American Concrete Institute, 2008
  13. Eurocode 8. Design Provisions for Earthquake Resistance of Structures. Brussels: European Committee for Standardization, 1994
  14. GB50010-2010. Design of Reinforced Concrete Structures. Beijing: Ministry of Housing and Urban-Rural Development, 2010
  15. Bonacci J, Pantazoupoulou S. Parametric investigation of joint mechanics. *ACI Structural Journal*, 1993, 90(1): 61–71
  16. Li B, Tran C T N, Pan T C. Experimental and numerical investigations on the seismic behavior of lightly reinforced concrete beam-column joints. *Journal of Structural Engineering*, 2009, 135(9): 1007–1018
  17. Hwang S J, Lee H J, Liao T F, Wang K C. Role of hoops on shear strength of reinforced concrete beam-column joints. *ACI Structural Journal*, 2005, 102(3): 445–453
  18. Murty C V R, Rai D, Bajpai K K, Jain S K. Effectiveness of reinforcement details in exterior reinforced concrete beam-column joints for earthquake resistance. *ACI Structural Journal*, 2003, 100(2): 149–156
  19. Bakir P G, Boduroğlu H M. A new design equation for predicting the joint shear strength of monotonically loaded exterior beam-column joints. *Engineering Structures*, 2002, 24(8): 1105–1117
  20. Haach V G, Lúcia Homce De Cresce El Debs A, Khalil El Debs M. Evaluation of the influence of the column axial load on the behavior of monotonically loaded R/C exterior beam-column joints through numerical simulations. *Engineering Structures*, 2008, 30(4): 965–975
  21. Hegger J, Sherif A, Roeser W. Nonseismic design of beam-column joints. *ACI Structural Journal*, 2003, 100(5): 654–664
  22. Feng D C, Xu J. An efficient fiber beam-column element considering flexure-shear interaction and anchorage bond-slip effect for cyclic analysis of RC structures. *Bulletin of Earthquake Engineering*, 2018, 16(11): 5425–5452
  23. Li B, Leong C L. Experimental and numerical investigations of the seismic behavior of high-strength concrete beam-column joints with column axial load. *Journal of Structural Engineering*, 2015, 141(9): 04014220
  24. Zhang P Z, Hou S, Ou J P. A beam-column joint element for analysis of reinforced concrete frame structures. *Engineering Structures*, 2016, 118: 125–136
  25. Feng D C, Ren X, Li J. Cyclic behavior modeling of reinforced concrete shear walls based on softened damage-plasticity model. *Engineering Structures*, 2018, 166: 363–375
  26. Feng D C, Ren X, Li J. Softened damage-plasticity model for analysis of cracked reinforced concrete structures. *Journal of Structural Engineering*, 2018, 144(6): 04018044
  27. Feng D C, Li J. Stochastic nonlinear behavior of reinforced concrete frames. II: Numerical simulation. *Journal of Structural Engineering*, 2016, 142(3): 04015163
  28. Hamdia K M, Silani M, Zhuang X, He P, Rabczuk T. Stochastic analysis of the fracture toughness of polymeric nanoparticle composites using polynomial chaos expansions. *International Journal of Fracture*, 2017, 206(2): 215–227
  29. Vu-Bac N, Lahmer T, Zhuang X, Nguyen-Thoi T, Rabczuk T. A software framework for probabilistic sensitivity analysis for computationally expensive models. *Advances in Engineering Software*, 2016, 100: 19–31
  30. Rabczuk T, Akkermann J, Eibl J. A numerical model for reinforced concrete structures. *International Journal of Solids and Structures*, 2005, 42(5–6): 1327–1354
  31. Rabczuk T, Belytschko T. Cracking particles: A simplified meshfree method for arbitrary evolving cracks. *International Journal for Numerical Methods in Engineering*, 2004, 61(13): 2316–2343
  32. Rabczuk T, Belytschko T. A three-dimensional large deformation meshfree method for arbitrary evolving cracks. *Computer Methods in Applied Mechanics and Engineering*, 2007, 196(29–30): 2777–2799
  33. Rabczuk T, Belytschko T. Application of particle methods to static fracture of reinforced concrete structures. *International Journal of Fracture*, 2006, 137(1–4): 19–49
  34. Rabczuk T, Bordas S, Zi G. On three-dimensional modelling of crack growth using partition of unity methods. *Computers & Structures*, 2010, 88(23–24): 1391–1411
  35. Rabczuk T, Zi G, Bordas S, Nguyen-Xuan H. A simple and robust three-dimensional cracking-particle method without enrichment. *Computer Methods in Applied Mechanics and Engineering*, 2010, 199(37–40): 2437–2455
  36. Rabczuk T, Eibl J. Numerical analysis of prestressed concrete beams using a coupled element free Galerkin/finite element approach. *International Journal of Solids and Structures*, 2004, 41(3–4): 1061–1080
  37. Rabczuk T, Zi G, Bordas S, Nguyen-Xuan H. A geometrically nonlinear three-dimensional cohesive crack method for reinforced concrete structures. *Engineering Fracture Mechanics*, 2008, 75(16): 4740–4758
  38. Sarsam K F, Phipps M E. The shear design of *in situ* reinforced concrete beam-column joints subjected to monotonic loading. *Magazine of Concrete Research*, 1985, 37(130): 16–28
  39. ACI-ASCE Committee 352. Recommendations for Design of

- Beam-Column Joints in Monolithic Reinforced Concrete Structures (ACI 352R-02). Farmington Hills: American Concrete Institute, 2002
40. Kwak H G, Filippou F C. Nonlinear FE analysis of RC structures under monotonic loads. *Computers & Structures*, 1997, 65(1): 1–16
  41. Hegger J, Sherif A, Roeser W. Nonlinear finite element analysis of reinforced concrete beam-column connections. *ACI Structural Journal*, 2004, 101(5): 604–614
  42. ABAQUS. ABAQUS Standard User's Manual, Version 6.9. Providence, RI: DassaultSystèmes Corp., 2009
  43. Feng D C, Wu G, Lu Y. Finite element modelling approach for precast reinforced concrete beam-to-column connections under cyclic loading. *Engineering Structures*, 2018, 174: 49–66
  44. Braconi A, Salvatore W, Tremblay R, Bursi O S. Behaviour and modelling of partial-strength beam-to-column composite joints for seismic applications. *Earthquake Engineering & Structural Dynamics*, 2007, 36(1): 142–161
  45. El-Tawil S, Sanz-Picon C F, Deierlein G G. Evaluation of ACI-318 and AISC (LRFD) strength provisions for composite columns. *Journal of Constructional Steel Research*, 1995, 34(1): 103–123
  46. Hajjar J F, Gourley B C. Representation of concrete filled steel tube cross-section strength. *Journal of Structural Engineering*, 1996, 122(11): 1327–1336
  47. Li B, Wu Y, Pan T C. Seismic behavior of nonseismically detailed interior beam-wide column joints-Part II: Theoretical comparisons and analytical studies. *ACI Structural Journal*, 2003, 100(1): 56–65
  48. Mahini S S, Ronagh H R. Numerical modelling of FRP strengthened RC beam-column joints. *Structural Engineering and Mechanics*, 2009, 32(5): 649–665
  49. Mirza S A, Hyttinen V, Hyttinen E. Physical tests and analysis of composite steel-concrete beam-columns. *Journal of Structural Engineering*, 1996, 122(11): 1317–1326
  50. Monti G, Spacone E. Reinforced concrete fiber beam element with bond-slip. *Journal of Structural Engineering*, 2000, 126(6): 654–661
  51. Sagbas G, Vecchio F J, Christopoulos C. Computational modeling of the seismic performance of beam-column subassemblies. *Journal of Earthquake Engineering*, 2011, 15(4): 640–663
  52. Sasmal S, Novák B, Ramanjaneyulu K. Numerical analysis of fiber composite-steel plate upgraded beam-column sub-assemblages under cyclic loading. *Composite Structures*, 2011, 93(2): 599–610
  53. Spacone E, El-Tawil S. Nonlinear analysis of steel-concrete composite structures: State of the art. *Journal of Structural Engineering*, 2004, 130(2): 159–168
  54. Lubliner J, Oliver J, Oller S, Oñate E. A plastic-damage model for concrete. *International Journal of Solids and Structures*, 1989, 25(3): 299–326
  55. Chen G M, Chen J F, Teng J G. On the finite element modelling of RC beams shear-strengthened with FRP. *Construction & Building Materials*, 2012, 32: 13–26
  56. Lin J P, Wu Y F, Smith S T. Width factor for externally bonded FRP-to-concrete joints. *Construction & Building Materials*, 2017, 155: 818–829
  57. GB/T50152–2012. Standard for Test Method of Concrete Structures. Beijing: Ministry of Housing and Urban-Rural Development, 2012
  58. Guo Z H. The Strength and Deformation of Concrete: Experimental Basis and Constitutive Models. Beijing: Tsinghua University Press, 1997
  59. Zhao X M, Wu Y F, Leung A Y T. Analyses of plastic hinge regions in reinforced concrete beams under monotonic loading. *Engineering Structures*, 2012, 34: 466–482
  60. Lin J P, Wu Y F. Numerical analysis of interfacial bond behavior of externally bonded FRP-to-concrete joints. *Journal of Composites for Construction*, 2016, 20(5): 04016028
  61. Chung Y S, Meyer C, Shinozuka M. Modeling of concrete damage. *ACI Structural Journal*, 1989, 86(3): 259–271
  62. Lee J, Fenves G L. Plastic-damage model for cyclic loading of concrete structures. *Journal of Engineering Mechanics*, 1998, 124(8): 892–900
  63. Comi C, Perego U. Fracture energy based bi-dissipative damage model for concrete. *International Journal of Solids and Structures*, 2001, 38(36–37): 6427–6454
  64. Shayanfar J, Akbarzadeh H. A practical model for simulating nonlinear behaviour of FRP strengthened RC beam-column joints. *Steel and Composite Structures*, 2018, 27(1): 49–74
  65. Fu J P, Zhang D C, Chen T, Bai S L. Experimental research on mechanics of force transmission and performance of shock-resistant joints with upper moderate shear-compression ratio. *Journal of Chongqing University (Natural Science Edition)*, 2005, 28(6): 84–90
  66. Fu J P, Chen X Y, Chen T, Bai S L. Experimental study on shock-resistant mechanism of frame joints with low to moderate shear-compression ratio. *Journal of Chongqing Architecture University (Natural Science Edition)*, 2005, 27(1): 41–47
  67. Zhang Y, Wang Z. Seismic behavior of reinforced concrete shear walls subjected to high axial loading. *ACI Structural Journal*, 2000, 97(5): 739–750
  68. Li P D, Wu Y F. Stress-strain model of FRP confined concrete under cyclic loading. *Composite Structures*, 2015, 134: 60–71
  69. Li P D, Wu Y F, Zhou Y W, Xing F. Cyclic stress-strain model for FRP-confined concrete considering post-peak softening. *Composite Structures*, 2018, 201: 902–915
  70. Quan C, Wang W, Zhou J, Wang R. Cyclic behavior of stiffened joints between concrete-filled steel tubular column and steel beam with narrow outer diaphragm and partial joint penetration welds. *Frontiers of Structural and Civil Engineering*, 2016, 10(3): 333–344
  71. Wu Y F, Hu B. Shear strength components in reinforced concrete members. *Journal of Structural Engineering*, 2017, 143(9): 04017092
  72. Hu B, Wu Y F. Quantification of shear cracking in reinforced concrete beams. *Engineering Structures*, 2017, 147: 666–678
  73. Hu B, Wu Y F. Effect of shear span-to-depth ratio on shear strength components of RC beams. *Engineering Structures*, 2018, 168: 770–783